FUNCTIONAL CIRCUITRY CONTROLLING THE SELECTION OF BEHAVIORAL PRIMITIVES IN *CAENORHABDITIS ELEGANS*

by

THEODORE LINDSAY

A DISSERTATION

Presented to the Department of Biology
and the Graduate School of the University of Oregon
in partial fulfillment of the requirements
for the degree of
Doctor of Philosophy

September 2012

DISSERTATION APPROVAL PAGE

Student: Theodore Lindsay

Title: Functional Circuitry Controlling the Selection of Behavioral Primitives in *Caenorhabditis elegans*

This dissertation has been accepted and approved in partial fulfillment of the requirements for the Doctor of Philosophy degree in the Department of Biology by:

Dr. William M. Roberts	Chair
Dr. Shawn R. Lockery	Advisor
Dr. Janis C. Weeks	Member
Dr. Tory G. Herman	Member
Dr. Michael C. Wehr	Outside Member

and

Kimberly Andrews Espy	Vice President for Research & Innovation/Dean of the Graduate School

Original approval signatures are on file with the University of Oregon Graduate School.

Degree awarded September 2012

DISSERTATION ABSTRACT

Theodore Lindsay

Doctor of Philosophy

Department of Biology

September 2012

Title: Functional Circuitry Controlling the Selection of Behavioral Primitives in *Caenorhabditis elegans*

One central question of neuroscience asks how a neural system can generate the diversity of complex behaviors needed to meet the range of possible demands placed on an organism by an ever changing environment. In many cases, it appears that animals assemble complex behaviors by recombining sets of simpler behaviors known as behavioral primitives. The crawling behavior of the nematode worm *Caenorhabditis elegans* represents a classic example of such an approach since worms use the simple behaviors of forward and reverse locomotion to assemble more complex behaviors such as search and escape.

The relative simplicity and well-described anatomy of the worm nervous system combined with a high degree of genetic tractability make *C. elegans* an attractive organism with which to study the neural circuits responsible for assembling behavioral primitives into complex behaviors. Unfortunately, difficulty probing the physiological properties of central synapses in *C. elegans* has left this opportunity largely unfulfilled. In this dissertation we address this challenge by developing techniques that combine whole-cell patch clamp recordings with optical stimulation of neurons. We do this using transgenic worms that express the light-sensitive ion channel Channelrhodopsin-2 (ChR2) in putative pre-synaptic neurons and fluorescent protein reporters in the post-synaptic neurons to be targeted by electrodes.

We first apply this new approach to probe *C. elegans* circuitry in chapter II where we test for connectivity between nociceptive neurons known as ASH required

for sensing aversive stimuli, and premotor neurons required for generating backward locomotion, known as AVA. In chapter III we extend our analysis of the *C. elegans* locomotory circuit to the premotor neurons required for generating forward locomotion, known as AVB. We identify inhibitory synaptic connectivity between ASH and AVB and between the two types of premotor neurons, AVA and AVB. Finally, we use our observations to develop a biophysical model of the locomotory circuit in which switching emerges from the attractor dynamics of the network. Primitive selection in *C. elegans* may thus represent an accessible system to test kinetic theories of decision making.

This dissertation includes previously published co-authored material.

CURRICULUM VITAE

NAME OF AUTHOR: Theodore Lindsay

GRADUATE AND UNDERGRADUATE SCHOOLS ATTENDED:

University of Oregon, Eugene
Marine Biological Laboratory, Woods Hole, Massachusetts
University of Minnesota, Minneapolis, Minnesota
Stonehill College, North Easton, Massachusetts

DEGREES AWARDED:

Doctor of Philosophy in Biology, 2012, University of Oregon
Bachelor of Science, 2000, Stonehill College

AREAS OF SPECIAL INTEREST:

Neurophysiology

PROFESSIONAL EXPERIENCE:

Graduate Teaching Fellow, Department of Biology, University of Oregon, Eugene, 2007-2012
Graduate Research Fellow, Department of Biology, University of Oregon, Eugene, 2006-2007
Junior Scientist, University Of Minnesota, Minneapolis, Minnesota, 2002-2005

GRANTS, AWARDS AND HONORS:

National Research Service Award (NINDS NS061697) 2010-2012

PUBLICATIONS:

Faumont, S., Lindsay, T. & Lockery, S. Neuronal microcircuits for decision making in *C. elegans*. *Current Opinion in Neurobiology* (2012).doi:10.1016/j.conb.2012.05.005

Lockery S.R., Hulme S.E., Roberts W.M., Robinson K.J., Laromaine A, Lindsay T.H., Whitesides G.M., Weeks J.C. A microfluidic device for whole-animal drug screening using electrophysiological measures in the nematode *C. elegans*. *Lab Chip* **12**, 2211–2220 (2012).

Goodman, M. B., Lindsay, T., Lockery, S. R. & Richmond, J. E. Electrophysiological methods for *Caenorhabditis elegans* neurobiology. *Methods Cell Biol.* **107**, 409–436 (2012).

Lindsay, T., Thiele, T. R. & Lockery, S. R. Optogenetic analysis of synaptic transmission in the central nervous system of the nematode *Caenorhabditis elegans*. *Nat Commun* **2**, 306–9 (2011).

Sevcik M.A.*, Jonas B.M.*, Lindsay T.H.*, Halvorson K.G., Ghilardi J.R., Kuskowski M.A., Mukherjee P., Maggio J.E., Mantyh P.W. Endogenous opioids inhibit early-stage pancreatic pain in a mouse model of pancreatic cancer. *Gastroenterology* **131**, 900–910 (2006).

Lindsay T.H., Jonas B.M., Sevcik M.A., Kubota K., Halvorson K.G., Ghilardi J.R., Kuskowski M.A., Stelow E.B., Mukherjee P., Gendler S., Wong GY., Mantyh P.W. A quantitative analysis of the sensory and sympathetic innervation of the mouse pancreas. *Neuroscience* **137**, 1417–1426 (2006).

Lindsay T.H., Jonas B.M., Sevcik M.A., Kubota K., Halvorson K.G., Ghilardi J.R., Kuskowski M.A., Stelow E.B., Mukherjee P., Gendler S., Wong GY., Mantyh P.W. Pancreatic cancer pain and its correlation with changes in tumor vasculature, macrophage infiltration, neuronal innervation, body weight and disease progression. *Pain* **119**, 233–246 (2005).

Sevcik M.A., Ghilardi J.R., Peters C.M., Lindsay T.H., Halvorson K.G., Jonas B.M., Kubota K., Kuskowski M.A., Boustany L., Shelton D.L., Mantyh P.W. Analgesic efficacy of bradykinin B1 antagonists in a murine bone cancer pain model. *J Pain* **6**, 771–775 (2005).

Halvorson K.G., Kubota K., Sevcik M.A., Lindsay T.H., Sotillo J.E., Ghilardi J.R., Rosol T.J., Boustany L., Shelton D.L., Mantyh P.W. A blocking antibody to nerve growth factor attenuates skeletal pain induced by prostate tumor cells growing in bone. *Cancer Res.* **65**, 9426–9435 (2005).

Sevcik M.A., Ghilardi J.R., Peters C.M., Lindsay T.H., Halvorson K.G., Jonas B.M., Kubota K., Kuskowski M.A., Boustany L., Shelton D.L., Mantyh P.W. Anti-NGF therapy profoundly reduces bone cancer pain and the accompanying increase in markers of peripheral and central sensitization. *Pain* **115**, 128–141 (2005).

Ghilardi J.R., Rorhrich H., Lindsay T.H., Sevcik M.A., Schwei M.J., Kubota K., Halvorson K.G., Poblete J., Chaplan S.R., Dubin A.E., Carruthers N.I., Swanson D., Kuskowski M., Flores C.M., Julius D., Mantyh P,W. Selective blockade of the capsaicin receptor TRPV1 attenuates bone cancer pain. *J. Neurosci.* **25**, 3126–3131 (2005).

Peters, C.M., Ghilardi, J.R., Keyser, C.P., Kubota, K., Lindsay, T.H., Luger, N.M., Mach, D.B., Schwei, M.J., Sevcik, M.A., Mantyh, P.W. Tumor-induced injury of primary afferent sensory nerve fibers in bone cancer pain. *Exp. Neurol.* **193**, 85–100 (2005).

Peters, C.M., Lindsay, T.H., Pomonis, J.D., Luger, N.M., Ghilardi, J.R., Sevcik, M.A., Manyh, P.W. Endothelin and the tumorigenic component of bone cancer pain. *Neuroscience* **126**, 1043–1052 (2004).

ACKNOWLEDGMENTS

I would first like to thank my advisor Shawn Lockery, who has not only provided me with the guidance and teaching necessary to achieve my degree, but who has also served as a staunch steward for scientific inquiry. Shawn has consistently required that his lab holds on to high standards of scientific rigor regardless of the current convention in the community. I would also like to thank all members of my committee who have provided me with wisdom and perspective. I would like to acknowledge the past and present members of the Lockery lab who have created a productive and fulfilling environment to complete my dissertation.

Finally I would like to acknowledge members Clay Spencer and Navin Pokala for providing us with unpublished strains.

This work was supported by funds provided to the lab by the National Institutes of Mental Health and National Science Foundation, as well as a pre-doctoral National Research Service Training Award from the National Institutes of Neurological Disease and Stroke.

DEDICATION

For my parents who have taught me the value of creativity and hard work.

TABLE OF CONTENTS

Chapter Page

LIST OF FIGURES

Figure Page

CHAPTER I

CHAPTER II

CHAPTER III

CHAPTER I

INTRODUCTION

BEHAVIORAL PRIMITIVES

Animals face a daunting task; they must obtain resources and mates, avoid predation, all while maintaining homeostasis in a complex ever-changing world. To overcome these challenges most animals are capable of executing a wide range of behaviors that allow them to adapt to environmental and homeostatic demands. Whereas these behaviors may equip the animal with the tools for success, they present the challenge of selecting and executing the appropriate behavior for a situation. This challenge is met — in large part — by the nervous system.

When presented with an environmental or homeostatic challenge, two options are available. The nervous system may invent the appropriate response *de novo*, or utilize previously learned and/or hard-wired or behaviors. The approach of drawing on pre-existing behaviors — known as behavioral primitives — appears to be widespread in the animal kingdom since it allows animals to build a range of more complex behaviors from a hierarchy of these simpler primitives [1-3].

In some instances, multiple primitives are executed simultaneously to generate a complex behavior. For example, there is evidence that the diversity of limb motions in tetrapods is accomplished through linear combination of circuits coding for a small subset motor programs known as muscle synergies [4,5].

In many instances however, simultaneous execution of more than one behavior is either impossible or maladaptive. For example an eye may only foveate a single target at a time [6,7], and flying insects need not generate the motor patterns for flight

and walking simultaneously [8]. In these instances the animal should select the correct behavior or sequence of behaviors in a way that is appropriate for the situation.

Mechanisms of flip-flops in neural systems

The selection between mutually exclusive behaviors can be thought of as a general model of decision making and has been studied in a range of animals including invertebrates, rodents and primates (Fig. 1). These studies have hinted that in many instances, the neural circuits responsible for the selection of behavioral primitives conform to an activity pattern known as a flip–flop. A flip–flop — which takes its name from the corresponding electrical circuit [9] — is inherently bi-stable, such that the underlying neurons, or groups of neurons are active or inactive for extended periods of time. Moreover, a key feature of flip–flops is that transitions between the active and inactive states are rapid when compared to the duration of the states themselves.

	Neural substrate	Circuit mechanism	Psychophysical assembly
Binocular Rivalry (Primate)	Histology	fMRI ↔ Perceptual report Extracellular electrophysiology ↔ Behavioral task	
Plume following (*B. mori*)	Dye tracing ↔ Intracellular electrophysiology Genetic identification	Extracellular electrophysiology	Tracking Tethered behavior
Locomotory Switching (*C. elegans*)	Genetic identification ↔ Calcium imaging ↔ Tracking Wiring diagram ↔ Intracellular electrophysiology		Computer vision

Figure 1: Experimental approaches for studying flip-flop circuits at three levels of organization. Three examples of putative flip-flop circuits that have been studied using a range of techniques. These techniques can be broadly categorized according to the level of organization they target. Arrows indicate instances where experiments have been performed that provide connections between multiple levels. This might occur when multiple techniques can be applied simultaneously in the same experiment, for example single unit recordings taken from monkeys trained to do a perceptual task while single unit recordings. Connections are also made when predictions from experiments or theory at one level are tested and validated and expanded on by experiments at another level. In this dissertation we test the predictions of the *C. elegans* wiring diagram using electrophysiology, and extend the diagram with functional data (red arrow).

There are multiple ways in which a nervous system can generate flip–flop behavior. One common mechanism is through the intrinsic voltage-dependent conductances of individual neurons.[9-11] In this case, a neuron is capable of sustaining constant depolarization for an extended period of time without support from external input. This type of depolarization is known as a plateau potential [12,13] and has been identified in many invertebrate and vertebrate systems [11,14,15]. The plateau potential in a single neuron might be able drive populations of follower cells and thus set the pace for a network-wide flip-flop pattern.

Theoretical considerations suggest that synaptic and network properties alone might also be able to support the generation of a flip–flop pattern. In this case, recurrent excitation or inhibition is thought to maintain stable active or inactive states across two or more neurons[16] Experimentally however, it has been considerably harder to identify instances where a flip-flop is demonstrably due to connectivity alone[9]. Here we focus primarily on just such examples where synaptic mechanisms are likely responsible for the generation of flip–flop behavior: the mating dance of the silkmoth *Bombyx mori*, perceptual switching between visual streams of the two eyes in primates known as binocular rivalry, and the locomotory switching of the nematode *C. elegans.*

Forming a comprehensive model across multiple levels of organization

In general, a particular experimental or theoretical technique is best suited to answer questions at a specific level of biological organization — certain techniques are appropriate for molecular or cellular questions whereas other are appropriate for studying cognitive or perceptual phenomena. The ongoing goal of research is to integrate findings drawn from these disparate sources into a comprehensive model; a

model that explains how the various levels of organization interdepend on each other. Of particular value to this goal is experimental or theoretical work that can establish links between levels of organization. Thus, in the discussion of neural flip-flops that follows, we pay particular attention to how what is known of neural systems informs such a comprehensive model (Fig. 1). Accordingly, we define three levels of organization to use as a framework for this discussion: (1) The neuronal substrate, (2) the circuit mechanisms, (3) the psychophysical assembly.

We consider the first level of organization, the neuronal substrate, to refer to the neurons and synaptic connectivity that are engaged during the execution of a particular behavioral primitive. Hence, the substrate of a flip-flop includes the circuitry that is necessary and sufficient for the primitives, and the circuitry whose activity is correlated with the primitives. Testing necessity usually involves experiments that determine if primitives are eliminated from animals when identified circuit elements are removed or otherwise rendered inactive. Establishing sufficiency usually involves experiments that manipulate identified circuit elements in a way that evokes the execution of the primitives of interest. Finally, determining if a neural circuit takes part in the natural generation of a primitive involves experiments that correlate activity patterns in a putative circuit with the production of the primitives. In summary, understanding the neuronal substrate necessarily includes an understanding the anatomical wiring of the circuit, but also requires an understanding of the neurochemistry and activity of neurons.

We consider the second level of organization, circuit mechanisms, to refer to the explanation of how the anatomic structure of the circuit and the tuning properties of the neurons are used to generate and select primitives. This often requires the formulation of models that make testable predictions. Testing these predictions then

requires experimental tools that can simultaneously measure the activity of multiple elements of the circuit and precisely manipulate neuronal activity.

We consider the third level of organization, psychophysical assembly, to refer to the explanation of how the flip-flop circuits are regulated by external input in order to meet the homeostatic and environmental demands placed on the organism. This often requires tools for quantitative behavioral analysis, methods to access hidden perceptual or neural states, and the precise control of sensory stimuli.

Ultimately, a comprehensive understanding of a flip–flop circuit and the corresponding primitives would encompass all three levels, and thus explain interdependence between the levels. For example, we would like to know how anatomic wiring explains the circuit mechanisms driving a neural computation. Likewise, we seek to understand how complex behaviors or cognitive function are assembled from the circuit mechanisms underlying the individual primitives.

MODEL SYSTEMS OF CIRCUIT LEVEL FLIP-FLOPS

Binocular rivalry in humans and non-human primates

A neural flip–flop may be critical to the formation of a coherent visual perception in humans and other non-human primates. Humans that are healthy, with normal binocular vision experience a single perception of the visual world, even though they receive two streams of visual information from the left and right eyes[17]. In most cases the binocular information is consistent, and thus the formation of a single coherent visual percept is not surprising; however, it was discovered that when the binocular patterns of visual information are inconsistent, a single visual perception of the visual world still forms [18,19]. The inconsistency between binocular visual streams

is resolved in some cases by fusing the two visual images into a single hybrid percept, and other cases by switching back-and-forth between the two discordant visual streams. This switching back-and-forth is known as binocular rivalry and suggests that a flip-flop circuit may participate in the formation of a single visual experience.

Most of our understanding of the neural substrate for binocular rivalry comes from work detailing the neuroanatomy of the visual pathways in general. Because binocular rivalry has traditionally been explored in animals that have sufficient cognitive function to report their perceptual experience (higher primates), rigorous lesion studies on these areas have not been performed for ethical reasons. Experiments using trans-cranial magnetic stimulation (TMS) to inactivate cortical regions in humans have suggested that disruption of V1 appears to alter the timing of rivalry intervals [20]. Unfortunately, TMS is a relatively low-resolution technique and limited to relatively superficial brain regions [21]. Thus it is difficult to target TMS to small, deep brain regions such as the monocular layers of the visual thalamus. This is a particular problem since inhibitory connectivity between the thalamic layers may themselves be critical to the mechanism of the flip–flop circuit [19].

There is considerable debate regarding how patterns of neural activity in different brain regions correlate with binocular rivalry. Single-unit recordings from non-human primates trained to report their perceptual experience have shown that successive stages of visual processing display increasing numbers of neurons that are modulated by binocular rivalry, with very few neurons in V1 or thalamus showing modulation and large number of neurons being modulated in the inferior temporal cortex [22,23] . In contrast to these reports, fMRI imaging studies have detected a BOLD

signature associated with binocular rivalry in early visual areas such as the thalamus and monocular regions of the visual cortex [24] .

The work delineating the visual system at the substrate level is key to understanding binocular rivalry at the level of circuit mechanisms. This is because different circuit mechanisms are plausible depending on where the perceptual rivalry is resolved [25,26]. In early stages of visual processing such as in the thalamus and visual cortex, neurons are tuned primarily to monocular stimuli, whereas in later stages neurons are tuned to binocular stimuli. Consequently, if the binocular conflict is resolved at early stages, the mechanism likely involves competition between the monocular visual streams through a process referred to as interocular completion [25,26]. Alternatively, if the perceptual conflict is resolved at later visual stages — where neurons show binocular tuning — it is expected that the mechanism involves competition between incompatible visual patterns, a model known as pattern completion. Multiple hybrid mechanisms have also been proposed; these mechanisms could involve excitatory feedforward pathways in which partial interocular completion would tip the scales for pattern completion in higher visual pathways. Likewise, feedback mechanisms are also possible in which higher visual areas are responsible for partially selecting a pattern, a process that would then be finalized by way of inhibitory feedback to early monocular areas [19].

At psychophysical assembly level, quite a bit is known about how binocular rivalry is regulated by environmental and stimulus parameters. Ever since the first rigorous psychophysical investigation of binocular rivalry by Wheatsone [18], it was recognized that the dominant perception switched randomly between eyes, and the statistics of this switching depended on the relative salience of the individual monocular stimuli: increased perceptual time was devoted to a stimulus that received better

illumination. Further studies have investigated the relationship between stimulus parameters and the temporal properties of the dominance intervals and have shown that a number of stimulus parameters such as contrast [27], motion, color [28] , spatial frequency [29,30] can influence the relative duration of the dominant or suppressed perception. Internal cognitive states such as attention also appear to have similar effects on the perceptual intervals.[31]

A common finding of all studies investigating the temporal properties of rivalry is that the perceptual intervals are fundamentally stochastic, thus stimulus and cognitive parameters exert their effects by modulating the statistics of the intervals, but the precise duration of any particular interval cannot be predicted [29] . Another conclusion of these studies is that some sort of adaptation process appears to influence the rate of switching between dominance intervals.[32]

Binocular rivalry represents an important example of a flip–flop circuit that may provide insight into visual awareness [33]. Unfortunately, the perceptual nature of this phenomenon has mostly limited the study primarily to primates. This has resulted in an understanding of the circuit that is very heavily weighted at the psychophysical assembly level. Models of the circuit mechanisms have been proposed, but neurophysiological experiments that directly test these models have yet to be reported [32]. Detailed tracing of the neuroanatomy and connectivity in the primate visual pathways have suggested a possible substrate for the flip–flop circuit, however this does not provide an exhaustive list of possible circuits, and unidentified connectivity may very well be critical for circuit function.

Mating dance of the silkmoth *B. mori*

Adult mail silkworm moths *B. mori* localize mates by tracking plumes of sex pheromones from conspecific females. Although moths exhibit this behavior both while flying and while walking, extensive studies of the behavior have focused primarily on walking. The behavior consists primarily of bouts of locomotion in a relatively constant direction interrupted by a back-and-fourth sequence of turning bouts. A series of experiments performed by the Kanzaki lab have indicated that a flip–flop circuit may be responsible for controlling the directionality and timing of the turns and loops during this behavior.

The neural substrate of this circuit has been localized primarily to a pair of bilaterally symmetric pre-motor regions of neuropil in the moth protocerebrum: the lateral accessory lobe (LAL) and the ventral protocerebrum (VPC). Olfactory input to these structures is thought to arrive by way of projection neurons emanating from the antenna lobes. The functional, anatomical and neurochemical properties of the neurons innervating the LAL and VPC neuropil have been studied by combining sharp electrode recordings, dye filling and immunohistochemistry respectively [34,35].

The suggestion of a flip–flop circuit was first made following recordings from a collection of descending interneurons that project from the LAL and VPC to ipsilateral neck motor neurons in the thoracic ganglia. Both the descending interneurons and the postsynaptic motoneurons displayed long trains of firing and quiescence with transitions between modes that occurred spontaneously and relatively quickly. Furthermore, these transitions events occurred both synchronously and asynchronously in the left and right LAL and VPC suggesting some sort of interconnectivity between hemispheres [36] .

A recent survey of 52 putative interneurons suggested a potential neural substrate for this interconnectivity. Using cytoarchetechture to distinguish presynaptic and postsynaptic regions of neuronal arborizations, the study identified a set of interneurons that appeared to connect contralateral LAL and VPC regions. Interestingly, some of these neurons displayed both flip–flop spiking patterns and GABA immunoreactivity, raising the possibility that these interneurons might supply reciprocal inhibition between the left and right elements of the circuit [37] .

At the circuit mechanism level, reciprocal inhibition has been proposed as a model to explain the flip–flop behavior of the circuit [38], however this has been difficult to test experimentally. It is possible that technical challenges associated with simultaneously recording and manipulating the activity of identified neurons in the moth has slowed progress towards validating these models [37]. For instance, a key test for reciprocal inhibition would involve activating the neurons of the LAL and VPC in one hemisphere and recording the predicted inhibition in the neurons of the contralateral hemisphere. This experiment has not yet been performed since, in order to identify the neurons of interest, large numbers of candidate neurons must be first impaled, and the tissue must be fixed for histology. Neither technique is compatible with robust pair-wise recordings *in vivo* [37]. Recent developments of transgenic approaches for identifying and labeling neurons in the *B. mori* nervous system may overcome some of these challenges so long as genetic reagents that target the cells of interest are identified [39].

At the psychophysical assembly level, the flip–flop circuit is thought to be control the turns associated with pheromone plume following for two reasons: (1) The neurons in the LAL and VPC project to neck motor neurons associated with steering the moths [38] (2) Pheromone stimulation can cause the activity in the projection neurons

to flip states [35]. Although *B. mori*, like other closely related moths, can follow pheromone plumes while in flight [40], the details of how the flip–flop circuit implements the behavioral algorithm used to follow a pheromone plume best understood in walking *B. mori*.

Behavioral studies of tethered and unrestrained walking *B. mori* have shown that the moths respond to phasic pheromone stimuli by initiating a turn to the left of right. Left-right antennal differences in stimulus concentration and onset times are used to direct the turn such that the moths steer into the plume. When the moth experiences a new phasic stimulus — leaving the plume for example — it will quickly switch into a new turn direction. In absence of a stimulus however, a turn may persist for extended periods of time, sometime causing the moth to loop before switching directions spontaneously [40]. Because the descending neurons of the LAL and VPC project to motor neurons responsible for steering, it is hypothesized that the persistence of these turns, and the rapid direction switching emerges from the bi-stable properties of the flip–flop circuit.

The putative flip–flop circuit in the *B. mori* protocerebrum may represent an important example of how a flip-flop can be used as the basis of a more complex search behavior — in this case it allows moths to navigate up the tortuous path of an airborne chemical plume. Significant progress has been made identifying a putative substrate for the circuit, and hypothetical circuit mechanisms and behavioral algorithms have been proposed. Nevertheless, a comprehensive understanding of the circuit has yet to be established. Experiments required to establish such an understanding would provide physiological evidence for the sign and strength of the proposed connections between circuit elements, measurements of neuronal activity

during pheromone following behavior, and manipulations of circuit activity in ways that test formal models of the circuit behavior.

Locomotory switching behavior of the nematode *C. elegans*

A third example of a putative neural flip-flop lies in the circuit controlling the forward-reverse direction of locomotion in the nematode *C. elegans*. Considerable work taking advantage of a wide range of experimental approaches has elaborated our understanding of the substrate, mechanisms and psychophysical assembly of this circuit.

A significant advance in our understanding of the neural substrate for the *C. elegans* locomotory circuit was provided by reconstructions from serial electron micrographs of 2.5 animals. By examining the location of presynaptic densities and gap junction connections on these micrographs White [41] and colleagues reconstructed a detailed map of the synaptic connectivity between the 302 uniquely identifiable neurons in the *C. elegans* nervous system. From these reconstructions White et al. noted a "striking grouping that is seen in interneurons ... whose synaptic outputs are directed primarily to motoneurons. These classes are AVA,AVB,AVD,AVE and PVC, which synapse onto motorneurons in the ventral cord." Of these 5 classes of neurons AVA and AVB have the most extensive connectivity with the ventral cord motorneurons[41]. Additionally, these two neuron classes are distinguished by the extensive number of inputs they receive from other neurons as well as from each other; they are both postsynaptic to more neurons, and receive a greater number of individual synaptic contacts than any other *C. elegans* neuron class [42]. This anatomical evidence suggests that AVA and AVB are uniquely poised to integrate external information from the rest of the *C. elegans* nervous system, and then use this information regulate locomotion via outputs to the motor system.

The necessity of the AVA and AVB class of neurons in the locomotory circuit was established by ablation studies which found that bilateral kills of AVA resulted in severely uncoordinated backward locomotion whereas bilateral kills of AVB resulted in uncoordinated forward locomotion. Similar, but less severe results were observed following ablation of the other premotor interneurons [43]. In accordance with the ablation results, these pre-motor interneurons are commonly identified as command neurons for the mode of locomotion they are necessary for: AVA,AVD, and AVE are the reverse command neurons and AVB and PVC are the forward command neurons.

Calcium imaging of several of these command neurons in unrestrained crawling worms has demonstrated that their activity patterns are consistent with their canonical assignment: AVA calcium is elevated during bouts of reverse locomotion and AVB calcium is elevated during bouts of forward locomotion [44-47]. Similar imaging studies have indicated that AVA and AVB generally share co-activity with their postsynaptic motoneuron targets, although this activity pattern can occasionally become decoupled, an effect that is exacerbated by mutations that effect the gap junctions between the pre-motor and motor system [46].

The mechanism for the flip–flop behavior of the locomotory circuit behavior has been the subject of considerable experimental and theoretical work. The suggestion that this circuit might represent a bi-stable switch was originally proposed when the necessity of the command neurons for locomotory behavior was first uncovered [43] however, whether this apparent bi-stability was intrinsic property of the command neuron network, or was driven by circuit mechanisms elsewhere in the *C. elegans* nervous system remained an open question.

Evidence that localized the source of bi-stability was first provided in a series of genetic experiments in which a mutated glutamate receptor was expressed in a subset of the command neurons [48]. This manipulation — which was presumed to result in chronic depolarization of the command neurons — had a profound effect on the duration of locomotory bouts, and worms flipped back-and-forth quickly between bouts of forward and reverse crawling. Because expression of the mutated receptor was restricted primarily to the command neurons, these results were taken as evidence that the flip–flop mechanism should be localized within command neuron circuit. The authors of this study proposed reciprocal inhibition between the forward and reverse pool of command neurons as a potential mechanism for the flip–flop behavior, though physiological evidence for this claim was notably absent.

Forward and reverse locomotion in *C. elegans* are particularly interesting examples of behavioral primitives that fall under the control of a flip–flop. This is because these primitives are assembled into a number of higher-oder behaviors. For instance, worms use bouts of reverse locomotion both to escape from aversive stimuli as well as to search for appetitive stimuli [49-56] . Both search and escape are thought to be assembled by way of regulation of the command neuron circuit through feed-forward synaptic pathways from sensory neurons[57,58] .

In the case of search behavior, the klinokenisis mechanism of chemotaxis to salts such as NaCl provides a clear example of how locomotory switching is used to navigate up a chemical gradient. By analyzing the movement of worms as they searched for the peak of a radial NaCl gradient, work in our lab has determined that worms monitor changes in salt concentration as they crawl, and use this to modulate turning frequency: turns are promoted when concentration is decreasing, and turns are suppressed when concentration is increasing [51,58]. Turning in this algorithm

implies an increase in reversal frequency because bouts of reverse locomotion result in changes in direction, and thus represent a major form of turning. Similar behavioral strategies have been identified with respect to chemotaxis to attractive olfactory[59], thermal and other environmental stimuli [60].

In the case of escape behavior, several types of aversive stimuli have been shown to trigger bouts of reverse locomotion. These include both harsh and light touch[50] as well as environmental vibrations that can be evoked with a tap to the petri plate housing the worms [61]. Additionally, aversive chemical stimuli such as the bitter tasting compound quinine or heavy metals such as copper will evoke a similar bout of reverse locomotion [53,62]. For large part, the sensory neurons responsible for transducing these aversive stimuli have been identified [50,63-65] and appear to signal to both the forward and reverse command neurons via monosynaptic and polysynaptic pathways [41].

The escape response to gentle anterior touch has been particularly well studied, and significant evidence for a synaptic pathway between the sensory neurons and the command neurons has been established through genetic and physiological experiments. The majority of these studies have indicated that the polymodal nociceptor ASH is primary responsible for sensing both bitter chemical stimuli and light touch, and ASH signals to the command neuron circuit via an excitatory pathway to the reverse command neuron AVA [50,62,66-69]. The physiological details of this pathway were uncovered in the work described in chapter II of this dissertation. The question of whether ASH signals to the forward members of the command neuron circuit such as AVB are answered in chapter III of this dissertation. The data collected in chapter III will be published as part of a separate report with the

coauthors Shawn Lockery, William Roberts, Tod Thiele, Navin Pokala, Rebecca Lindsay, Kristy Lawton, Cornelia Bargmann and Steven Augustine.

A number of experimental approaches have coalesced to inform our understanding of the *C. elegans* locomotory flip-flop, hinting at the possibility that it might be possible to form a comprehensive model of this circuit that spans all three levels of organization. However, before such a comprehensive model is formed there are notable experimental and theoretical gaps that must be addressed. In particular, extending the wiring diagram to include physiological data on the sign and dynamics of putative connections would allow circuit mechanisms to be reconciled with the neural substrate in a coherent framework.

With a single exception [69], direct physiological demonstration of synaptic connectivity in the central nervous system of *C. elegans* has been notably absent until the recent development of tools for stimulating genetically identified neurons with pulses of light [70,71]. These tools allow electrophysiological investigation of connectivity between pairs of neurons using a single electrode so long as light sensitive ion channel can be expressed in the pre-synaptic neurons of interest. This allows experiments to be performed that would previously require two simultaneous electrical recordings, a challenging task given the small size of *C. elegans* neurons.

Along with several other labs [72,73], we developed techniques for combining optogenetic simulation with electrophysiology to examine synaptic connectivity between *C. elegans* neurons. We describe development of this procedure in chapter II which has been published with co-authors Tod Thiele and Shawn Lockery. We then applied this technique to the locomotory flip–flop and physiologically established reciprocal inhibitory connectivity between AVA and AVB. We also applied

the technique to study how this flip–flop is regulated by nociceptive stimuli by testing for connectivity between ASH and both AVA and AVB. Finally, we used our physiological observations to build a model of a simplified circuit that is sufficient to explain the flip–flop behavior of the circuit, and the emergent locomotory behavior. This dissertation contains a description of these experiments.

CHAPTER II

OPTOGENETIC ANALYSIS OF SYNAPTIC TRANSMISSION IN THE CENTRAL NERVOUS SYSTEM OF THE NEMATODE *C. ELEGANS*

This work was published in volume 2 of the journal Nature Communications in May 2011. I along with Shawn Lockery and Tod Thiele designed experiments. Tod Thiele assisted with the generation of strains. Shawn Lockery and I wrote the manuscript. I collected and analyzed the data.

INTRODUCTION

Any method for synaptic physiology between identified neurons should allow for selective stimulation of the presynaptic neuron, quantitative control of presynaptic activation, and positive identification of the postsynaptic neuron. In many systems, these requirements can be met by making pairwise whole-cell patch clamp recordings. Such pairwise recordings are challenging in any system, but in *C. elegans* the challenge is compounded by the fact that whole-cell patch clamp recordings from individual neurons are comparatively short-lived. In genetically tractable organisms, however, the first two requirements can now be met using an optogenetic approach in which a photoactivatable ion channel is genetically targeted to the desired presynaptic neurons[71,74-76]. The third requirement can be met by targeting the expression of fluorescent proteins to the desired postsynaptic neurons[77].

To develop such a method in *C. elegans*, we focused on the connection between the neuron classes ASH and AVA. ASH is a left-right pair of glutamatergic, nociceptive sensory neurons [50,64,66,78-80]. Anatomical reconstructions imply that ASH makes monosynaptic and polysynaptic connections onto AVA, a left-right pair of premotor

command interneurons that expresses at least two types of glutamate receptors[41,43,48,68,81]. Our selection of the ASH-AVA connection was based on three main considerations. First, there is ample physiological evidence that the connection is functional as mechanical and optical stimulation of ASH elicits inward synaptic currents and calcium transients in AVA, respectively[69,82]. Second, ASH makes monosynaptic connections onto AVA. Third, the connection is behaviorally relevant, as ASH neurons respond to stimuli that elicit escape responses[79], and AVA neurons are required for, and active during, reverse locomotion[43,44], an inherent component of escape behaviors in *C. elegans*.

Here we present a method for recording quantitatively evoked synaptic currents and potentials at central synapses in *C. elegans* for the first time. ChannelRhodopsin-2 (ChR2) is used to photoactivate[71] presynaptic neurons and the whole-cell patch-clamp configuration is used to record from postsynaptic neurons. To demonstrate the utility of the new methodology, we analyzed synaptic correlates of AVA-mediated escape responses. We found that the time course of excitatory synaptic currents in AVA closely matched the time course of the probability of escape behavior. Evoked currents were surprisingly complex, exhibiting three distinct components. The two main components increased smoothly as stimulus strength was increased, suggesting that the overall input-output function of AVA-mediated escape responses is graded. This result is consistent with a model in which the energetic cost of escape behaviors in *C. elegans* is tuned to the intensity of the threat.

RESULTS

Optogenetics, dissection, and neuronal identification

To activate presynaptic neurons, we created a transgenic strain (XL165) in which ChR2, tagged with yellow fluorescent protein (YFP), is expressed under the control of

the sra–6 promoter. This promoter was chosen because it has the greatest known specificity for ASH neurons. As expected from published *sra-6* expression patterns[80], we observed strong ChR2 expression in ASH and weak ChR2 expression in ASI, a left-right pair of chemosensory neurons required for diet-induced longevity, dauer formation, regulation of reverse locomotion, and chemotaxis[83-85]; we refer to ASH and ASI collectively as "*sra-6* expressing neurons." Although photostimulation is likely to activate both pairs of neurons, the synaptic current attributable to ASI is likely to be small relative to the current attributable to ASH because of the difference in expression levels.

The effectiveness of photostimulation was assessed in whole-cell patch clamp recordings from ASH (Fig. 1a,b), which revealed an inward current with the transient and sustained components that are characteristic of this probe[43]. The amplitude and time course of the photocurrents were functions of stimulus irradiance, consistent with previous results in other systems[76], as well as muscles and other neurons in *C. elegans*[75,86]. Photostimulation failed to elicit currents in worms grown in the absence of all-trans retinal, the essential cofactor[71] for ChR2, indicating that native light sensitivity in *C. elegans*[87,88] did not contribute to the currents recorded in ASH neurons at the irradiances used here.

The two standard methods for exposing *C. elegans* neurons for patch clamp recording[48,89,90] involve large incisions in the cuticle and a sudden release of internal pressure, either of which might disrupt synaptic connections. We found that the preparation's physical integrity could be preserved to a greater degree by a new dissection procedure in which a tiny slit, less than 10 μm in length, is made immediately adjacent to the target neuron (AVA). In most instances, only a single neuron emerges from the slit. To facilitate this procedure, we manipulated worms

before dissection into grooves formed in an agarose surface using a microfabricated mold (Fig. 1c) and glued them in place such that the worm's cuticle was convex at the point nearest to the target neuron.

Postsynaptic neurons were identified for patch clamp recording by transgenic expression of a red fluorescent protein (RFP) which is visualized by green light. Although we also tried green fluorescent protein (GFP) for this purpose, we found that the likelihood of observing evoked synaptic currents was much lower than when RFP was used, presumably because the blue light used to visualize GFP depresses synaptic transmission by sustained excitation of ChR2. Postsynaptic neurons were identified by expression of the RFP known as tdTomato[91] under the control of the *nmr-1* promoter, which labels the command neuron AVA, its nearest neighbor AVE, and four other interneurons that are further away[48].

Although AVA and AVE can be distinguished, in principle, by the relative positions of their somata, it was not always possible to discern which neuron emerged from the slit. However, inspection of the amplitude and time course of the current families measured in voltage clamp when either of the two neurons may have been exposed revealed two qualitatively distinct physiological types: one having small currents that activated almost instantaneously and decayed quickly, and the other having large currents that activated and decayed more slowly (Fig. 1d). We also noted that the whole-cell capacitance in recordings of the first type was systematically larger than the whole cell capacitance in the second type (0.77±0.02 pF vs. 0.53±0.02 pF; $p < 0.001$). This result suggested that the first type corresponds to AVA neurons, whose only neurite is twice as long as AVE's[41]. We confirmed this correspondence by recording from a transgenic strain in which AVA could be identified positively as the only neuron that expressed both a red and a green fluorescent protein

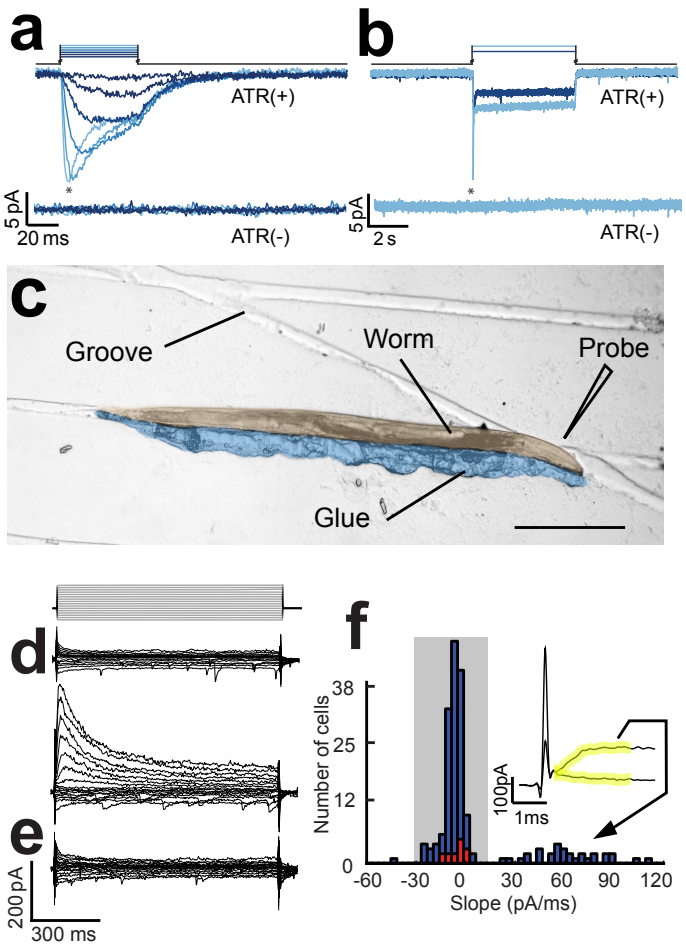

Figure 1. Photostimulation of ASH neurons and electrophysiological identification of AVA neurons. (**a**) Membrane current evoked by photostimulation of ASH neurons with 50ms long stimuli; asterisks denote the transient component of the current. The stimulus irradiance varied from 0.07 to 12.5 mW/mm^2 in steps of 1.04 log units. (**b**) membrane current in ASH neurons in response to 5s long pulses of light at 0.75 and 12.5 mW/mm^2. Upper and lower current traces are from animals supplied (ATR+) or not supplied (ATR-) with all-*trans* retinal, respectively. Holding potential was -55 mV. (**c**) A glued-worm positioned for dissection on a micropatterned agarose substrate. The worm and glue have been pseudocolored to enhance contrast. Scale bar = 200µm. (**d**) Representatives of the two types of current families obtained when recording from from unidentified command neurons presumed to be either AVA or AVE as identified by cell body position and expression of tdTomato driven by the *nmr-1* promoter. Voltage steps ranged from -80 mV to +40 mV in steps of 10 mV from a holding potential of -55 mV as shown above. (**e**) A current family from an AVA neuron positively identified by combinatorial expression of dsRed and GFP driven by the for *glr-1* and *rig-3* promoters, respectively. The voltage protocol was the same as in **d**. (**f**) Histogram of the slope of the initial current in response the +40mV voltage step in a population of 182 unidentified neurons that were either AVA or AVE (blue bars) and 10 neurons positively identified as AVA by combinatorial expression. Slope was computed over the 2 ms window (yellow) following termination of the capacitative transient ; the inset shows typical traces during this window for the two types of current families shown in **d**. Shading indicates the subpopulation of neurons identified *post hoc* as AVA.

marker (Fig. 1e,f). Henceforth, we identified AVA by its unambiguous physiological characteristics alone, using the initial slope of the membrane current as shown in Fig. 1f.

Escape responses elicited by photostimulation

Before trying to record synaptic currents in AVA neurons in the strain XL165, we tested whether AVA neurons are likely to exhibit synaptic responses in this strain by attempting to elicit escape responses via photostimulation. These experiments were done using the so-called glued-worm preparation[56,92], in which the worm is glued by the head to an agarose-coated coverslip and bouts of reverse locomotion ("reversals") are scored manually by noting the direction of propagation of undulatory wavesalong the worm's body. To ensure that photostimulation was the same as in the electrophysiological experiments recounted below, we performed the behavioral assays in our patch clamp setup, using its light source and microscope objective for photostimulation. As expected, reversal bouts occurred stochastically[51,93] before, during, and after photostimulation (Fig. 2a). However, plotting the change in the probability of reverse locomotion versus time (Fig. 2b) revealed clear increases in probability for two of the three stimulus strengths used; the third stimulus was apparently too weak to elicit detectable behavior. Because AVA makes a major contribution to reversals[43], these results provided some assurance that synaptic responses would be seen in patch clamp recordings from AVA.

Synaptic currents in AVA neurons

To investigate the relationship between synaptic input to AVA and the time course of reversal responses, we recorded synaptic currents in AVA in response to light pulses that matched the duration and irradiance of the light pulses used in the behavioral

experiments of Fig. 2a,b. Synaptic currents elicited by photostimulation were inward (Fig. 2c), consistent with the fact that ASH is a glutamatergic neuron and AVA is known to express ionotropic glutamate receptors and to exhibit an inward current in response to direct application of glutamate in dissected preparations[48,69,81]. It should also be noted that laser ablations of ASI indicate that it normally acts to suppress reversal behavior[85], suggesting that inward currents we observed in AVA are attributable solely to ASH. This fact, together with the above-mentioned contrast between ChR2 expression levels in ASH and ASI, suggests that the effect of ASI activation is at most a modest reduction in the amplitude of this inward current. Thus, photostimulation of *sra-6* expressing neurons appears to be a reasonable approximation to photostimulation of ASH alone.

Synaptic currents in AVA were remarkably well correlated with reversal behavior (measured in different animals) in three important respects. First, currents were observed in response to the two stimuli that were behaviorally sufficient, whereas currents were absent in response to the only stimulus that was behaviorally insufficient. Second, the stimulus that elicited the strongest behavioral response also elicited the strongest synaptic response. Third, the overall duration of the currents matched the duration of the behavioral responses. We conclude that synaptic current in AVA is well correlated with reversal probability.

Further inspection of AVA synaptic currents revealed three phenomenologically distinct components. The first component ("onset transient," Fig. 2c, asterisks) was a short latency current that decayed rapidly. Synaptic latency, measured relative to the onset of the light pulse (see Methods), was a decreasing function of stimulus irradiance (Supplementary Fig. 1). The peak amplitude of the onset transient was an increasing function of stimulus irradiance as shown by the current-irradiance (C-I) plot in Fig. 3a. The second component ("sustained current," Fig. 2c, red trace) was a

long-lived current identified in the figure by median filtering of the membrane current. To quantify this component, we computed its average during the time period corresponding to the rising phase of the behavioral responses shown in Fig. 2b ($0 \leq t \leq 2.1$ s); it too was found to be an increasing function of irradiance (Fig. 3b). The third component ("unitary event frequency", Fig. 2c, insets) was a transient increase in the frequency of small, unitary synaptic currents. The effect on this component of increasing stimulus irradiance was not statistically significant (Fig. 3c). We conclude that the onset and sustained components of the synaptic current observed in response to photostimulation are graded functions of stimulus strength. Evidence for graded synaptic connectivity between ASH and AVA.

As we understand the term, a "graded synaptic connection" is one in which action potentials are required neither for transmitter release nor for postsynaptic signaling, and incremental changes in membrane potential in the soma of the presynaptic neuron cause incremental changes in membrane potential in the soma of the postsynaptic neuron[94].

This term can be applied to monosynaptic connections and to so-called functional connections, which are defined in terms of the net effect of multiple synaptic pathways, including parallel pathways that may also be polysynaptic. The signature of a graded synaptic connection is a smoothly rising input-output function, defined by the curve obtained when postsynaptic membrane potential is plotted against presynaptic membrane potential. Conversely, the signature of a non-graded is an input-output function that exhibits a step-like discontinuity, indicating a distinct threshold for synaptic transmission.

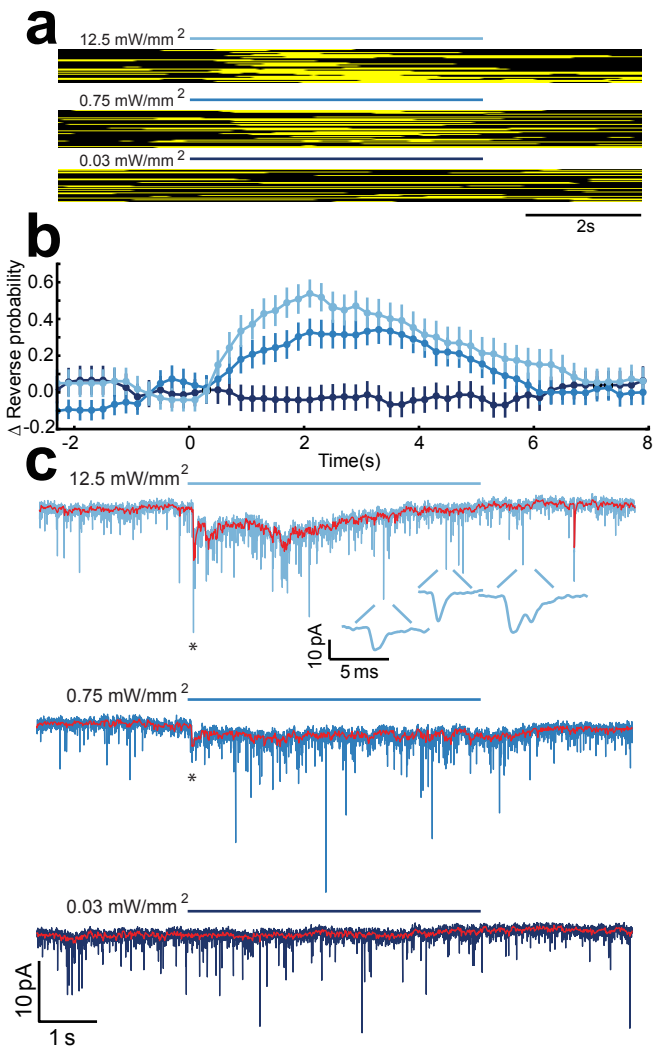

Figure 2. Time course of reversal behavior and the synaptic current in AVA evoked by photostimulation of *sra-6* expressing neurons. (**a**) Raster plots showing the behavioral state of semi-restrained worms in response to photostimulation at three different irradiances. Black and yellow pixels indicate forward and reverse swimming, respectively. Blue bars show the time of the photostimulus at the indicated irradiance. (**b**) The stimulus evoked change in the probability of reverse swimming for the data shown in **a**. Error bars are SEM (n > 42 for each stimulus condition). (**c**) Typical synaptic current in AVA evoked by photostimulation of *sra-6* expressing neurons at the three irradiances shown in **a**. Holding potential was -55 mV. Three phenomenologically distinct components of the response are visible: the onset transient (asterisk), the sustained current (red trace showing median-filtered current), and the increase in the unitary event frequency(insets). Data in **a-c** are plotted on the same time axis to facilitate comparison of the time course of behavior and synaptic current.

To delineate the approximate input-output function of the connection between ASH and AVA, we recorded voltage responses in these neurons when ASH was stimulated by an increasing series of brief (50 ms) light pulses. We found that the amplitudes of responses of ASH and AVA to photostimulation were increasing functions of stimulus irradiance and lacked any discontinuities that might suggest non-graded synaptic transmission. This relationship held for presynaptic depolarizations in ASH (Fig. 4a,b), postsynaptic currents in AVA (Fig. 4c,d) and postsynaptic potentials in AVA (Fig. 4e,f). Discontinuities were also absent when, combining data from both experiments, we plotted postsynaptic membrane potential against presynaptic membrane potential (Fig. 4g), in accordance with the definition of a graded synaptic connection. Together, these data are consistent with a graded functional synaptic connection between ASH and AVA. This finding agrees with previous reports of graded synaptic transmission between neurons in the nematode *Ascaris suum* and at the neuromuscular junction in *Ascaris suum* and *C. elegans*[86,88,95,96].

The design of the experiment in Fig. 4 also allowed us to compare the time course of synaptic currents and synaptic potentials in AVA neurons, albeit in different animals. It is interesting to note that average synaptic potentials outlasted average synaptic current evoked by the same photostimulus (Fig. 4c vs. e). Temporal filtering by passive membrane properties of AVA neurons was not sufficient to account for this discrepancy, as the average predicted membrane time constant of AVA neurons was 0.85±0.03 ms (see Methods). This result suggests that synaptic potentials in AVA may involve one or more types of sustained postsynaptic mechanisms. Possibilities include cellular-level mechanisms such as current through NMDA receptors expressed in AVA neurons[48] or network level mechanisms such as positive feedback via recurrent excitatory synaptic connections[41]. Further experiments will be required to distinguish between these possibilities.

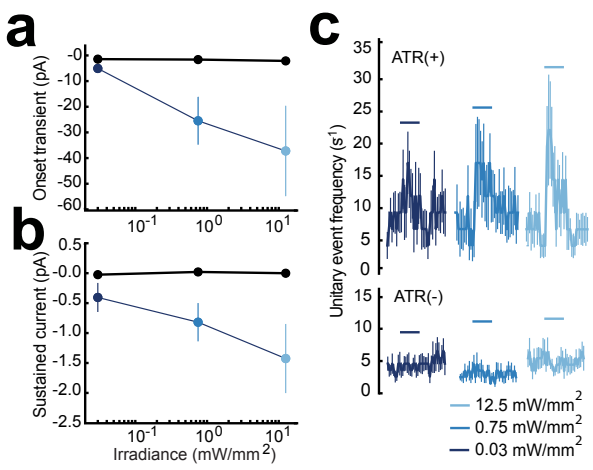

Figure 3. Quantitative summary of the three components of the synaptic current in AVA evoked by photostimulation of *sra-6* expressing neurons. Currents were quantified and subjected to an ANOVA to test for a linear relationship with irradiance. (**a**) Peak onset transient synaptic current vs. irradiance in animals supplied with all-*trans* retinal, (ATR(+),blue dots, n = 9) and retinal-free controls, (ATR(-),black dots, n = 4). The magnitude of the onset transient from ATR(+) animals increased significantly with stimulus irradiance (p=0.029) (**b**) Average sustained synaptic current vs. irradiance. Current was averaged over the interval $0 \leq t \leq 2.1$ s. Symbols as in **a**. The magnitude of sustained currents from ATR(+) animals increased significantly with stimulus irradiance (p= 0.044) (**c**) Average time course of the frequency of unitary synaptic events in response to photostimulation at three different irradiances (horizontal blue bars). The frequency of unitary synaptic events evoked by photostimulaion increased with stimulus irradiance in ATR(+) animals, but this effect did not reach significance (ANOVA, p= 0.246). Upper and lower traces show data from animals supplied or not supplied with all-*trans* retinal, respectively. ATR(+) n = 9, ATR(-) n=4. Error bars (**a-c**) are SEM. Statistics (**a-c**): within-subjects ANOVA test for a linear trend.

Distinguishing between chemical and electrical transmission

Gap junctions, the anatomical correlates of electrical synapses, are commonly encountered in the reconstructions of *C. elegans* central nervous system[41]. To test whether the synaptic current between *sra-6* expressing neurons and AVA contains an electrical component, we attempted to record synaptic currents in mutant worms in which classical chemical synaptic transmission is known to have been essentially eliminated by a loss-of-function mutation in the gene *unc-13*. This gene encodes the nematode form of MUNC-13, which is required for the priming and release of clear-

core vesicles characteristic of synapses that utilize glutamate and other classical neurotransmitters[97,98]. We found that all three components of the synaptic current evoked by photo-simulation of *sra-6* expressing neurons were absent in *unc-13*(e51) mutants (Fig. 5), leading us to conclude that pathways comprised of purely electrical synapses do not make a detectable contribution to evoked synaptic currents in AVA. We also found that the *unc-13*(e51) mutation eliminated the spontaneous events seen in the baseline periods before photostimulation (Fig. 5a,b,d), indicating that these events too are synaptic in origin. Together, these findings are consistent with the fact that the *C. elegans* neuronal connectivity database shows that there are only a few all-electrical synaptic pathways from *sra-6* expressing neurons to AVA and all of them are highly indirect (fifth order or higher)[41] . The absence of evoked synaptic currents in *unc-13* mutants does not, of course, rule out a contribution from polysynaptic pathways that contain both chemical and electrical synapses.

In addition to clear-core synaptic vesicles, *C. elegans* neurons also contain so-called dense core vesicles, which release catecholamines and neuropeptides[99]. Although ASH is not known to express synthetic enzymes for catecholamines[100], it does express genes for at least four neuropeptides, and neuropeptide gene expression is also seen in neurons that are members of the polysynaptic pathways between ASH and AVA . To test whether a component of the synaptic current in AVA might involve the release of dense-core vesicles, we recorded synaptic currents in mutants in which this release mechanism has been impaired by a deletion (e928) in the gene *unc-31*, which is required for all dense core vesicle release in *C. elegans*[101,102]. Although we observed a trend toward reduction of synaptic currents across all three components (Fig. 5), the effect failed to reach significance for any individual component. We conclude that there might be a modest

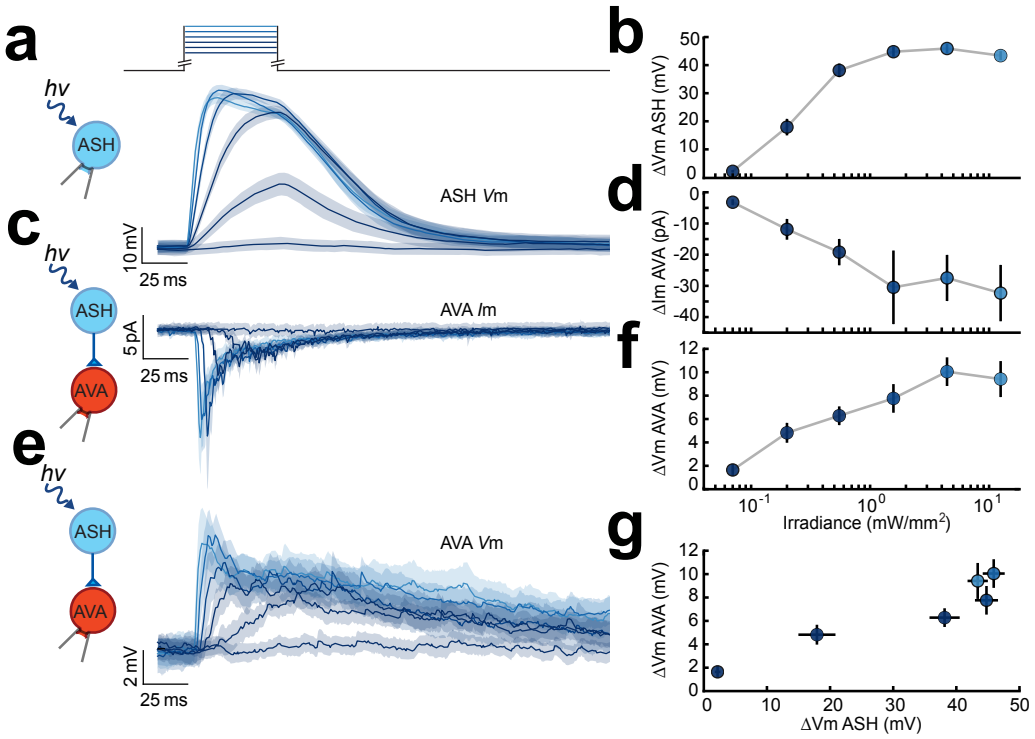

Figure 4. Evidence for graded synaptic transmission between *sra-6* expressing neurons and the command neuron AVA. (**a**) Average membrane potential of ASH neurons in response to the photostimulation protocol shown at the top. Color indicates stimulus irradiance which varied from 0.07 to 12.5 mW/mm^2 in steps of 1.04 log units. (**b**) Peak depolarization evoked in ASH vs. irradiance (n=14 in **a,b**). (**c**) Average membrane current in AVA neurons (photostimulation as in **a**). (**d**) Peak synaptic current evoked in AVA vs. irradiance (n=9 in **c,d**). (**e**) Average membrane potential in AVA neurons (photostimulation as in **a**). (**f**) Peak synaptic potential vs. stimulus irradiance (n=18 in **e,f**). data were recorded from the indicated neuron but in different animals. (**g**) Postsynaptic membrane potential in **f** plotted against presynaptic membrane potential in **d**. SEM is indicated by gray bands in **a,c,d**, and error bars in **b,d,f,g**.

requirement for UNC-31 in synaptic signaling between ASH and AVA, suggesting a possible role for peptides and catecholamines as neurotransmitters or neuromodulators. A similarly mild effect has been observed in null mutants of the analogous gene in Drosophila[103].

Evidence for glutamate transmission

Candidate glutamatergic synapses in *C. elegans* can be identified using genetic evidence for presynaptic expression of the glutamate vesicular transporter gene eat-4[78], together with postsynaptic expression of NMDA or non-NMDA glutamate receptor subunits[81,104]. One such candidate is the monosynaptic connection from ASH to AVA. The observation that AVA neurons exhibit inward currents in response to exogenously applied glutamate[69,81] supports this view. However, glutamatergic synapses are likely to play a central role in polysynaptic connections as well. Indeed, by combining the *C. elegans* neuronal wiring diagram with published expression patterns of eat-4 and various glutamate receptor subunits[78,105] , we found that 62 of the 72 polysynaptic pathways (up to fourth order) between ASH and AVA contain at least one connection that is a candidate glutamatergic synapse.

As a direct test of whether glutamatergic transmission is required for the connectivity between ASH and AVA, we first measured the peak current-voltage relationship of the synaptic currents elicited in AVA by photostimulation of *sra-6* expressing neurons (Fig. 6a,b). We found that synaptic currents reversed near 0 mV, the value obtained in recordings from AVA neurons in dissected preparations in response to exogenous glutamate[69]. We next recorded synaptic currents in the combined presence of the glutamate antagonists CNQX and MK-801. We found that glutamate antagonists reduced the amplitude of all three components of the AVA synaptic current Fig. 6c-f.

Together, these findings lead us to conclude that the overall connectivity between ASH and AVA is at least partly glutamatergic. The persistence of synaptic currents in the presence of glutamate antagonists may reflect a glutamate-independent component of the synaptic current or incomplete access of the antagonists to the central nervous system. The latter might be expected because the hole formed in the cuticle during dissection is small and likely to be partially occluded by surrounding soft tissue.

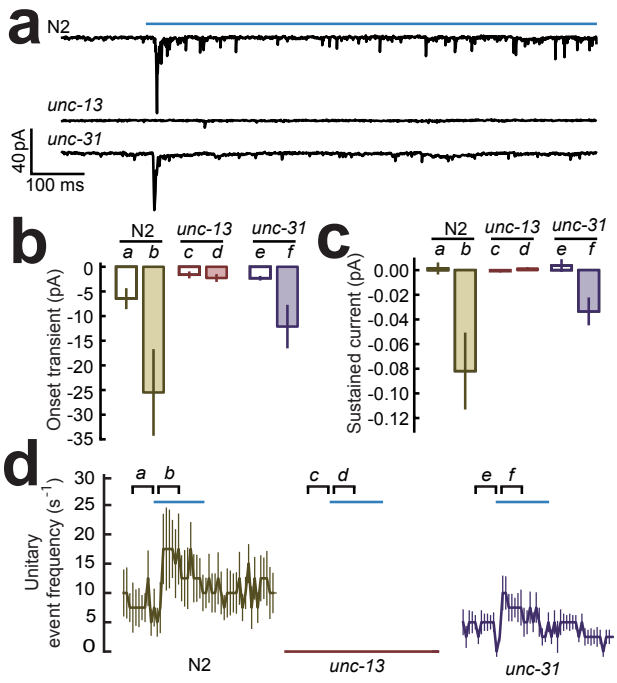

Figure 5. Synaptic currents evoked by photostimulation of *sra-6* expressing neurons in two synaptic transmission mutants. (**a**) Typical currents in wild type (N2) animals and animals with mutations in synaptic transmission mediated by clear-core vesicles (*unc-13(e51)*) or dense-core vesicles (*unc-31(e928)*). The photostimulus is shown by the blue bar above the top trace. (**b**) Summary of effects on the onset transient. The *unc-13* mutation eliminated the onset transient (*b* vs. *d*, $p = 0.002$) whereas the *unc-31* mutation did not have a significant effect (*b* vs. *f*, $p = 0.2978$). (**c**) Summary of effects on the sustained current. The *unc-13* mutation eliminated the sustained current (*b* vs. *d*, $p = 0.00025$) whereas the *unc-31* mutation did not have a significant effect (*b* vs. *f*, $p = 0.652$). (**d**) Summary of effects on frequency of unitary events relative to stimulus onset in wild type. The *unc-13* mutation essentially eliminated the increase in unitary event frequency (*b* vs. *d*, $p = 0.0002$) whereas the *unc-31* mutation did not have a significant effect (*b* vs. *f*, $p = 0.037$). Statistics (**b-d**): Bonferroni-adjusted Mann-Whitney U test. The joint level of significance (α) in the Bonferroni adjustment was 0.017 in **b**, and 0.025 in **c**, **d**. Sample sizes were: wild type, $n=9$; *unc-13* $n=10$; and *unc-31,* $n=10$. Error bars are SEM.

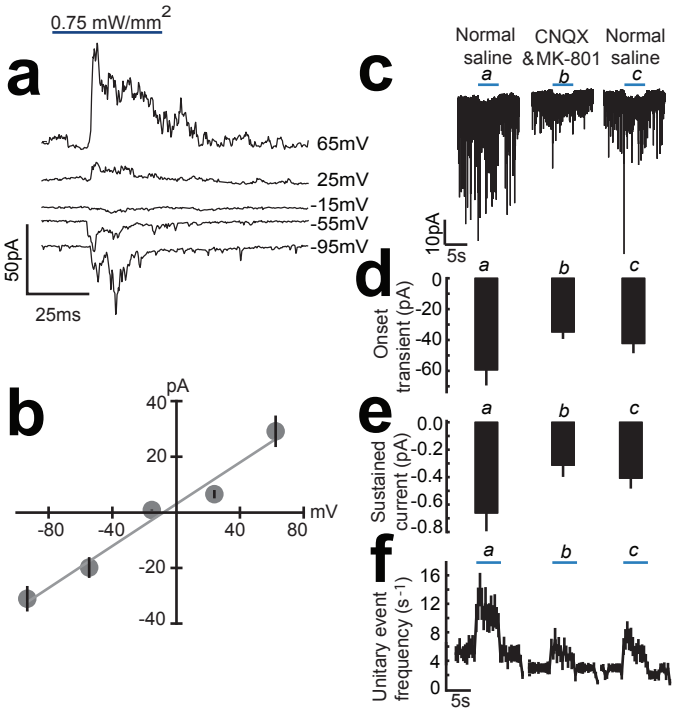

Figure 6. Evidence for glutamatergic synaptic transmission between *sra-6* expressing neurons and AVA. (**a**) Reversal of synaptic currents in AVA by clamping the neuron at holding potentials from -95 mV to +65 mV. (**b**) Peak synaptic current versus holding potential in 10 AVA neurons. A linear fit indicates a reversal potential of -7.0±3.2 mV. (**c**) Typical spontaneous and evoked synaptic currents recorded from AVA in normal saline, during the bath application of glutamate blockers CNQX (200 µM) and MK-801 (50 µM), and following washout with normal saline. The photo stimulus is indicated by the blue bar. (**d**) Glutamate blockers reduced the average onset transient during the stimulus (pooled *a*,*c* vs. *b*, p=0.0009; *a* vs. *c*, p = 0.622). (**e**) Glutamate blockers reduced the average sustained current during the stimulus (pooled *a*,*c* vs. *b*, p=0.0007; *a* vs. *c*, p = 0.575). (**f**) Glutamate blockers reduced the average unitary event frequency during the stimulus (pooled *a*,*c* vs. *b*, p=0.003; *a* vs. *c*, p = 0.375). Statistics (**d**-**f**): within-subjects ANOVA (n = 10) with orthogonal planned comparisons. The joint level of significance (α) was 0.025 throughout. Error bars are SEM.

DISCUSSION

Although the present combination of photostimulation and patch clamp electrophysiology ("photo-electrophysiology") has been used effectively in studies of synaptic transmission at the *C. elegans* neuromuscular junction[74,86], it has not been applied to synapses of the central nervous system in *C. elegans* until now. A key feature of the new method is a minimally invasive dissection procedure designed to

increase the likelihood that synaptic connections remain intact after the cell body of the postsynaptic neuron is exposed for recording. This procedure was facilitated by gluing the animals in close-fitting groves formed by a microfabricated mold.

The main limitation of photo-electrophysiology in *C. elegans* is the current scarcity of pairs of promoters that are entirely specific for the presynaptic and postsynaptic neuron classes of interest. Fortunately, this limitation is at least partly surmountable. In cases in which unwanted presynaptic neurons express the photoprobe, it may be possible to identify the presynaptic neuron by the relative position of its cell body and to simulate it selectively using patterned illumination such as that provided by a digital mirror device[82]. In cases in which unwanted postsynaptic neurons are labeled, we have shown that ambiguities can sometimes be resolved using electrophysiological criteria such as the amplitude and time course of membrane current. Restriction of expression patterns using a combinatorial expression system[105,106] is another option for addressing this limitation.

An alternative method for determining functional connectivity in *C. elegans* is "all-optical interrogation" which also employs optogenetic techniques to activate (or inactivate) presynaptic neurons, but uses calcium imaging rather than electrophysiology to monitor postsynaptic neurons[82]. All-optical interrogation is probably better suited for a large-scale, first-pass examination of functional connectivity in which it is advantageous to investigate several pairs of neurons in a single preparation. Other advantages include the ability to resolve activity in subcellular compartments and to preserve both internal milieu and whole-animal behavior. Photo-electrophysiology is probably better suited for situations in which calcium concentration is an inappropriate proxy for membrane potential or synaptic current. Such situations include separation of the effects of membrane currents from

the effects of synaptic currents, as well as the detection and analysis of synaptic inhibition, other subthreshold events, synaptic events that occur on the time scale of milliseconds to tens of milliseconds, and the latency of synaptic transmission. Other advantages include the ability to manipulate cellular and synaptic physiology by altering a neuron's internal or external milieu.

The anatomical connectivity of the nervous system of the nematode worm *C. elegans* has been reconstructed completely[41]but the signs and strengths of its synaptic connections are almost entirely unknown. Photo-electrophysiology should greatly accelerate the process of annotating the neuronal wiring diagram. Indeed, we used the new approach to characterize the net physiological effects *sra-6* expressing neurons upon the command neuron AVA. The functional connection between these neurons and AVA exhibits three components: an onset transient, a sustained current, and an increase in unitary event frequency. We found that all three components are sensitive to glutamate antagonists. In perhaps the simplest interpretation of these findings, the onset transient and the sustained current are the result of temporal summation of the unitary currents, such that all three components are manifestations of a single synaptic mechanism. Under this interpretation, the fact that glutamate blockade is incomplete is explained by incomplete access of the antagonists to the central nervous system, but our experiments do not, of course, exclude the possibility that additional synaptic mechanisms are involved.

The conclusion that the functional connection between ASH and AVA is graded is complicated by the possibility that although expression of ChR2 in ASI neurons in XL165 worms is weak, it might be sufficient to generate a significant amount of synaptic current in AVA. If so, it is formally possible that the connection between ASH and AVA is not graded, i.e., it is a step-function whose effect is balanced by

inhibitory effects of the functional connection between ASI and AVA. Although the ASI-AVA connection is likely to be inhibitory as the model requires, we think this scenario is unlikely because the it would require that the effect of ASI-AVA connection to be greatest when ASI is least activated (Fig. 7).

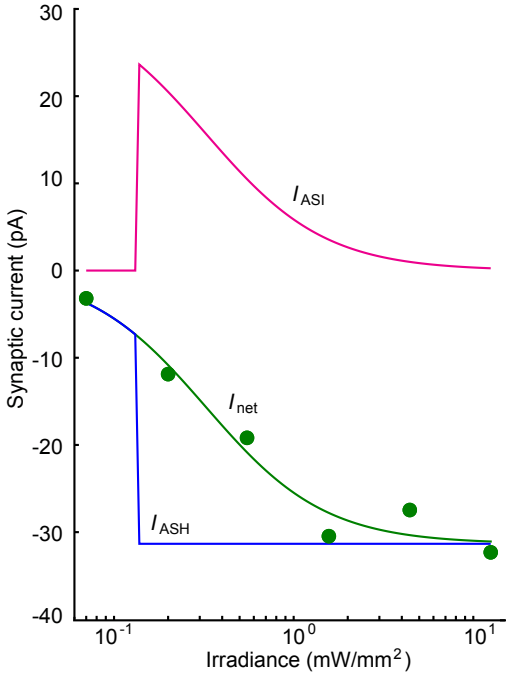

Figure 7. Hypothetical current-irradiance curve for the functional connection between ASI and AVA. The model assumes that ASI inhibits AVA (i.e., currents attributable to ASI are greater than or equal to zero at all irradiances), which is justified by the fact that ablation of ASI neurons causes an increase in reversal frequency[85]. The model also assumes, counterfactually, that the current-irradiance curve for the connection between ASH and AVA (blue) is a step-function (i.e., the connection is not graded). I_{ASI}, the predicted curve for the ASI connection (magenta) was computed by subtracting the step function I_{ASH} from I_{net} (green), the overall current-irradiance curve obtained experimentally.

Graded synaptic transmission between ASH and AVA is consistent with a model in which stronger – and likely more dangerous – aversive stimuli elicit a greater number of stochastic escape responses per unit time. As energetic cost almost certainly increases with the number of escape responses, graded transmission

between ASH and AVA may exist to provide a means of reserving the most costly responses for the most dangerous stimuli.

METHODS

Animals

The strains used in this study were wild-type *C. elegans* Bristol (N2), MT7929 *unc-13*(e51); CB169 *unc-31*(e169); XL157 ntIs29[*nmr-1*::tdTomato], XL153 ntIs27[*sra-6*::ChR2*YFP,unc-122::dsRed], XL165 ntIs2[*sra-6*::ChR2*YFP,unc-122::dsRED]; ntIs29[*nmr-1*::tdTomato], XL167 *unc-31*(e928);ntIs27[*sra-6*::ChR2*YFP,unc-122::dsRED];ntIs29[*nmr-1*::tdTomato], XL168 *unc-13*(e51);ntIs27[*sra-6*::ChR2*YFP,unc-122::dsRED];ntIs29[*nmr-1*::tdTomato]. NC1749 otEx239[(*rig-3*::GFP), pha-1(e2123)III]; hdIs32[*glr-1*::DsRed2] was a gift from Clay Spencer and David Miller[107].

Molecular biology

The *sra-6*::ChR2*YFP construct was made by first inserting the *sra-6* promoter into the xba-1 site of the pPD95.75 Fire Vector[108]. ChR2*YFP was then inserted between the BamHI and EcoRI site of pPD95.75 3' of the promoter. The p*sra-6*[80] and ChR2*YFP[2] were obtained as clones of preexisting constructs. The *nmr-1*::tdTomato plasmid was made by first inserting tdTomato between the BamHI and EcoR1 sites of pPD95.75. 5Kb of the *nmr-1* promoter and the first 5 codons of the predicted *nmr-1* protein coding sequence[48] were amplified from genomic DNA by PCR and inserted between the sphI and salI to fuse tdTomato with the first 5 codons of *nmr-1* in the pPD95.75 vector. All constructs were injected at 50 ng/µL using published methods[108].

Photostimulation

Worms were photostimulated in both the behavioral and electrophysiological experiments using the blue channel (470 nm) of a dual wavelength LED module (Rapp OptoElectronic, Hamburg, Germany) that was focused by a 63x 1.4 NA oil immersion objective lens (Zeiss, part number 440762-9904). Irradiance was determined by measuring the power emitted from the objective using an optical power meter placed above the front lens of the objective (Newport, Irvine, Ca) and dividing by the area of the field of illumination at the focal plane of the preparation.

Electrophysiology

Worms were prepared for electrophysiology by gluing them to an agarose pad formed on a coverslip that became the bottom of the recording chamber as described in [89]. Here, however, the pad contained grooves (cross-section 20 μm x 20μm) formed by pressing a microfabricated polydimethylsiloxane (PDMS) mold[109] into a drop of molten agar to produce an obliquely crossed array (Fig. 1c). To ensure that the pad adhered to the coverslip and not to the mold, the coverslip was pre-coated with a thin layer of agarose that was allowed to dry before forming the pad. Prior to gluing, each worm was positioned with its body in one groove and the tip of its head in a second groove that intersected the first one. As a result, the neck region was bent slightly to one side, producing a convex surface at the point of contact between the dissecting probe and the body; this arrangement applies tension to the worm's cuticle to facilitate entry of the sharp glass probe used for dissection. In addition, the worm was rotated so that its ventral midline was at the bottom of the first groove, placing the target neuron at the most favorable latitude for dissection. The chamber was filled with external saline and the cell body of the neuron was exposed by making a small slit in the cuticle. Recording pipettes were pulled and pressure-polished[109] to achieve resistances of 10–20 MΩ when filled with normal internal

saline. Voltage and current-clamp recordings were made with a modified Axopatch 200A[89] amplifier. Pulses used to calculate whole-cell capacitance and series resistance were filtered at 50 kHz and sampled at 125 kHz. Voltage clamp current families, and recordings of photostimulation-evoked events, were filtered at 2 kHz and sampled at 10 kHz.

Physiological solutions

Internal saline consisted of (in mM): 125 K-gluconate ,1 $CaCl_2$, 18 KCL, 4 NaCl, 1 $MgCl_2$, 10 HEPES, 10 EGTA, pH 7.2 (KOH). External saline consisted of 5 KCl, 10 HEPES, 8 $CaCl_2$, 143 NaCl, 30 glucose, pH 7.2 (NaOH).

Behavioral analysis

Worms were prepared for behavioral experiments[56] and care was taken to ensure that the conditions of behavioral and electrophysiological experiments were closely matched. Briefly, each worm was glued by the head to an agarose-coated coverslip that formed the bottom of the recording chamber. The preparation was submerged in external physiological saline and positioned on the stage of the inverted microscope normally used for patch clamping and photostimulation; thus, the same microscope objective (63x) and light source were used in both types of experiments. Whole-worm behavior was recorded (29.97 FPS) using a video camera attached to a 4x objective stationed above the preparation; the camera was fitted with a long-pass emission filter to prevent the ChR2 excitation light from reaching the camera. Behavioral state (forward or reverse) was scored off-line by noting the direction in which undulatory waves propagated along the worm's body; the scorer was blind to the timing and irradiance of the stimulus as well as the experimental treatment (± all-trans retinal). The time course of the probability of each state was obtained by

aligning the behavioral records of different animals to stimulus onset and computing bin-wise averages of the fraction of time spent in each state across animals.

Data analysis and statistics

Whole cell capacitance and series resistance were estimated from the currents evoked by a voltage pulse from -40 to -70 mV[89]. Briefly, after seal formation, we measured uncompensated electrode capacitance and seal resistance in the on-cell configuration before rupturing the patch to obtain the whole-cell configuration. The effects of uncompensated electrode capacitance the current across the seal resistance were removed by subtracting on-cell currents from whole-cell currents before further analysis. The time constant of AVA neurons was estimated as the product of whole-cell capacitance and resistance. Series resistance errors were compensated offline. We excluded cells that had a whole-cell capacitance of less than 0.2 pF, or a holding current at -55 mV that was outside the range of -40 pA to 20 pA, as these cells were likely to be damaged. In current-clamp experiments, we excluded cells in which the resting potential was less negative than -50 mV.

Components of synaptic current

The onset transient was quantified as the peak inward current observed during the first 50 ms of the photostimulus minus the peak current observed in the 50 ms immediately before the stimulus. The sustained component of the synaptic current was quantified as the average median-filtered current during the initial 2.1 s of the stimulus minus the average current during an equivalent period immediately before the photostimulus. The frequency of unitary events was defined in terms of events detected using a weighted least squares fit of a scaled template.[110] For this component, synaptic response was defined as the frequency of unitary currents

during the stimulus minus the frequency of unitary events during equivalent period immediately before the photostimulus. Analyses were performed using custom software written using IgorPro™ or the ScyPy[111] Python libraries. Error bars represent ± standard error of the mean (SEM).

CHAPTER III

MINIMAL NEURONAL CIRCUITRY FOR LOCOMOTORY SWITCHING BEHAVIOR IN *C. ELEGANS*

This chapter contains data collected as part of a project modeling the behavioral kinetics of worm locomotion. This model, known as the stochastic-switch-model, predicts the reciprocal connectivity between the command neurons from the behavioral statistics of worm locomotion. Thus, the data presented here will be published as part of the stochastic-switch-model with the coauthors Shawn Lockery, William Roberts, Tod Thiele, Navin Pokala, Rebecca Lindsay, Kristy Lawton, Cornelia Bargmann and Steven Augustine. The model discussed in this chapter intends to analyze the electrophysiological data from a biophysical perspective and is separate from the stochastic-switch-model.

INTRODUCTION

C. elegans locomotory behavior is largely restricted to movement along its body axis in either the anterior (forward) or posterior (reverse) direction. Analysis of *C. elegans* tangential movement has shown that instead of occupying many different forward or reverse velocities, worms have preferred gates[45,51,93,112]. With the exception of brief pauses at zero velocity, transitions between these gates happen in a roughly all-or-non manner [113,114]. Thus, these gates represent mutually exclusive modes of locomotion.

Early studies of the neural circuitry controlling locomotory behavior found that laser ablation of the pre-motor interneuron class AVA resulted in worms with severe defects in reverse locomotion, whereas ablation of the pre-motor interneuron class AVB resulted in analogous defects in forward locomotion [43]. This led to the

hypothesis that AVA and AVB serve as command neurons for reverse and forward locomotion respectively. Inspection of the anatomical reconstructions of the worm nervous system — known as the wiring diagram — supports the command neuron hypothesis [41]. The wiring diagram indicates circuity that is segregated at the level of command neuron output: projections from AVA are nearly exclusively to the motor neurons thought to generate reverse thrust, and projections from AVB are to motor neurons thought to generate forward thrust [41].

Further support for the command neuron hypothesis comes from calcium imaging of AVA and AVB in unrestrained crawling worms; calcium was found to be elevated in AVA throughout bouts reverse locomotion, and depressed throughout bouts of forward locomotion [44-47]. The converse pattern was found in AVB [45,46]. These imaging experiments not only further solidify the role of AVA and AVB as command neurons, but also speak to the nature of the control system: since the command neurons are active during mutually exclusive behaviors, their activity must also be mutually exclusive. Although voltage in AVA and AVB has not been recorded simultaneously, we infer that AVA is only active when AVB is inactive and vise versa. We refer to these segregated patterns of activity as flip-flop behavior.

The neural mechanisms that generate the flip-flop behavior in the *C. elegans* command neuron circuit are unknown, but several possibilities exist. Two prominent possibilities include intrinsic bi-stability of the command neurons, and/or emergent properties of the synaptic network [9,115-117].

Both mechanisms beg the questions of what connectivity exists between the two neurons and how sensory neurons regulate the system. In the case that the command neurons are intrinsically bi-stable, then some synaptic interaction is

required so that the neurons do not remain co-active or co-inactive for extended periods. In the case that the patterns are an emergent property of the network, then is there a minimal circuit that allows for both stability of the patterns and transitions between them? In either case, sensory input might be directed at AVA, AVB or both cells, and the consequences of this input on network behavior would depend highly on the intrinsic properties of the neurons and their interconnectivity.

Inspection of the wiring diagram indicates that monosynaptic contacts are made reciprocally between the AVA and AVB class (Fig. 1). Additionally, the wiring diagram also suggests extensive poly-synaptic connectivity [41]. In spite of the anatomical evidence, this putative synaptic connectivity has not been tested at the physiological level, thus it is not known if it is functional, let alone if it is excitatory or inhibitory.

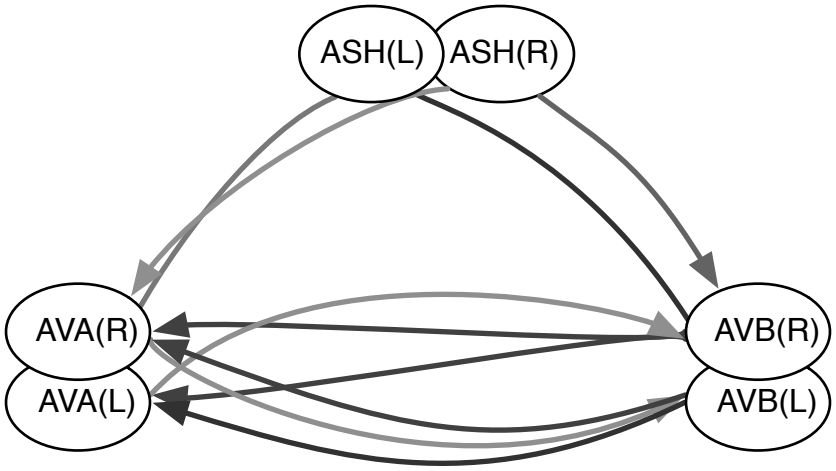

Figure 1. Anatomical predictions for circuitry involved in the regulation of the command neuron circuit. Diagram shows putative monosynaptic connections between the left and right members of three neuron classes ASH,AVA, and AVB. Darker arrows indicate a greater number of synaptic contacts associated with the connection. Left-right laterality is indicated in parenthetically.

The ASH nociceptive neuron class presents a useful way to uncover the mechanisms of how sensory input regulates the command neuron circuit. ASH is known to trigger a bout of reverse locomotion when it detects nociceptive stimuli at the anterior end

of the worm. It has already been well established that this response results in part via excitatory synaptic output to AVA [50,62,66-69,73,78,82,118] but the wiring diagram also indicates extensive monosynaptic (Fig. 1) and polysnaptic pathways from ASH to AVB [41]. Yet, again the functionality and sign of this connectivity between ASH and AVB has not been tested.

Here, we first study the intrinsic properties of the command neurons and then test the functionality of putative synaptic connectivity between pairs of neurons. To test for connectivity we use a recently developed method that involves photo-activating a putative presynaptic member of a neuron pair using the light-gated ion channel Channelrhodopsin-2 (ChR2) [70,71], and recording the evoked synaptic currents in the other class [72,73,118]. By measuring the reversal potential of the synapse we determine if this connectivity is excitatory or inhibitory.

In this study, first we establish that the command neuron membrane properties are largely passive. Second, we show that inhibitory reciprocal connectivity exists between the forward and reverse command neurons. Third, we show that inhibitory connectivity exists between the nociceptor ASH and AVB. Finally, we use our observations of command neuron intrinsic properties and connectivity to formulate a biophysical model. This model is sufficient to produce activity patterns consistent with the production of worm locomotory behavior.

In the description of experiments focused on synaptic connectivity in this study, we adopt the following nomenclature to help clarify the directionality of a particular connection of interest: we append (pre) to the names of putative presynaptic neurons and (post) to the names of putative postsynaptic neurons.

RESULTS

The membrane currents of the AVA and AVB command neurons are largely passive

Prior recordings from the AVA command neurons have shown that AVA have a predominantly linear current-voltage relationship compared to other *C. elegans* neurons [116]. Because of these passive properties in AVA, it is unlikely that intrinsic bi-stability in AVA is necessary for the formation of the network-wide flip-flop behavior. To our knowledge whole cell recordings from the AVB neurons have not performed, thus it remains possible that intrinsic bi-stability in AVB serves as a source of the network-wide behavior.

To study the intrinsic properties of AVB, we first focused on targeting AVB for electrical recordings. Traditionally, this targeting in *C. elegans* involves expressing a fluorescent reporter protein under the control of a cell- or class-specific promotor [89,119]. Unfortunately, no truly specific promotor for the AVB class of neurons has been identified [105]. Fortunately, in prior studies we were able to employ semi-specific promoters for this identification procedures so long as additional anatomic and/or electrophysiolgical exclusion criteria could be applied [118].

We selected the *sra-11* promotor as the best candidate for targeting AVB since it was shown to express in only three cell classes: AVB, AIY and AIA [105,120]. Furthermore, the anatomy of these three cell classes indicated that they might be easily distinguished during recording procedures; the somata are well separated and AVB have long primary neurites that descend the length of the body. In contrast AIY and AIA have short primary neurites restricted to the anterior nerve ring [41].

When we expressed the red fluorescent protein tdTomato using the *sra-11* promotor we found that indeed we were able to successfully target AVB using anatomical criteria alone. We then asked if the currents evoked by depolarizing voltage steps in AVB were consistent with intrinsic regenerative behavior. We found that like the forward command neuron AVA, the current-voltage relationship in AVB is mostly linear (Fig. 2a,b). Additionally, again like AVA, depolarizing voltage steps from AVB did not evoke currents with slowly activating and inactivating kinetics. Both of these observations support a passive model of AVA and AVB intrinsic properties [121], and distinguish these command neurons from many other identified *C. elegans* neuron classes such as ASE(R), [89], ASH [65] (Fig. 2c), AWC [122], AFD, AWA [123], RIM [116], AIY [119] and AVE [118].

The AVA and AVB neurons are reciprocally inhibited

Having the means to record from the postsynaptic member of the putative AVA(pre) to AVB(post) connection, we next focused on testing for synaptic connectivity between these neuron classes. Before doing so, however, we needed to be able to selectively activate the presynaptic member of this pair. The *rig-3* promoter expresses in the AVA neuron class, thus by using this promotor to express ChR2 we were able to activate AVA(pre) with pulses of blue light. Recordings from AVA in this strain validated that ChR2 activated excitatory currents as expected (data not shown).

Finally, to test for connectivity, we constructed worms expressing ChR2 in AVA(pre) and tdTomato in AVB(post) using the promotors listed above. Furthermore, because short wavelength light has been reported to engage non-specific effects on the wild type *C. elegans* locomotory circuit, we expressed these constructs in a background in

which the non-specific effect of blue-light stimulation is eliminated by a mutation (ce314) of the *lite-1* gene [87].

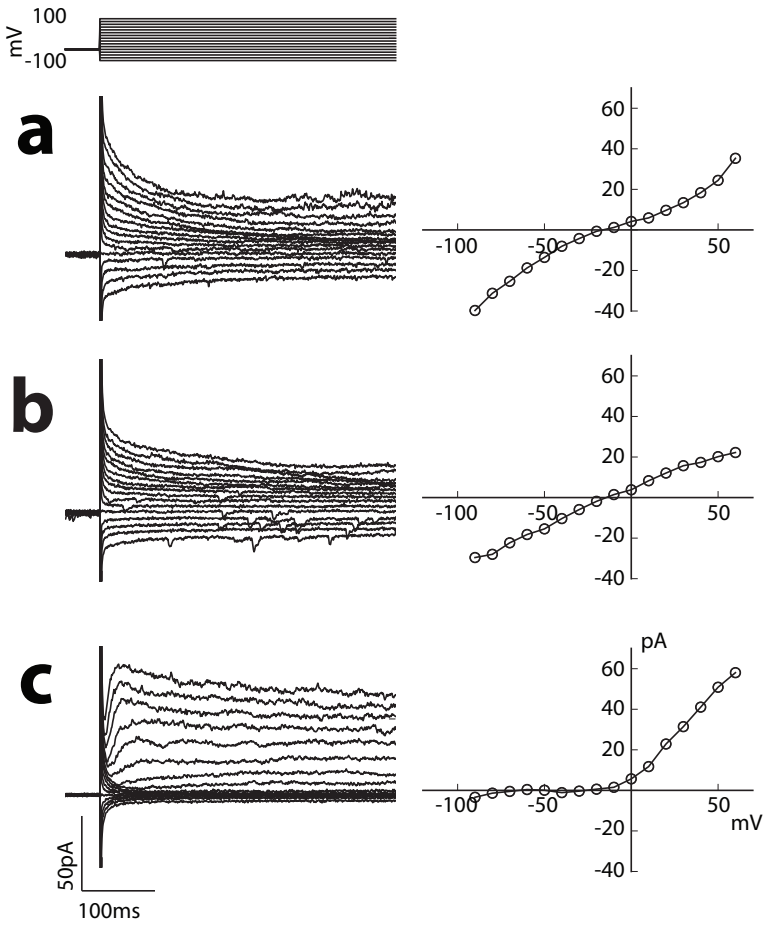

Figure 2. Comparison of intrinsic currents in the AVA and AVB command neurons with the ASH sensory neuron. (**a-c**) Example recordings from AVA **a**, AVB **b,** and ASH **c,** showing the first 600ms of a family of membrane currents evoked by voltage steps from -80 to +40mV in steps of 10mV. The current-voltage relationship for these families is shown to the right. The same voltage protocol was used for **a-c**, top.

To simultaneously determine the magnitude (conductance) of putative functional connectivity from AVA(pre) to AVB(post), and also measure the sign (reversal

potential) we voltage-clamped AVB(post) at a family of membrane potentials and recorded the currents evoked by photostimulation of AVA(pre) (Fig. 3a). To estimate the reversal potential of observed connectivity, we first estimated the conductance of the connection in a given preparation by fitting the relationship between the light-evoked current and holding potential with a linear (ohmic) model (Fig. 3b). We tested the fit against the null hypothesis of zero conductance. In a small subpopulation of preparations (4/33), photostimulation AVA(pre) evoked a statistically significant synaptic conductance (Fig. 3b,c). It is unknown why some preparations failed to exhibit significant synaptic conductances however, we suspect this is likely due to disruption of network connectivity during the dissection and immobilization procedure. Thus, we view the preparations that display a significant synaptic conductance as a more accurate representation of the connectivity of an intact worm. Hence, we excluded preparations with a conductance that was not significantly different than zero, and then calculated the group-wise reversal potential as the average zero-current intercept of the linear fits across the remaining preparations.

Using this exclusion method, we calculated average reversal potential of the AVA(pre) to AVB(post) connectivity to be -69.51± 3.57 mV (Fig. 3c). This reversal potential is roughly consistent with a chloride conductance (calculated chloride equilibrium = -77.6 mV), however we acknowledge the formal possibility of a mixed synaptic conductance. Nevertheless in intact worms, we expect that this conductance to yield an inhibitory synaptic effect in AVB(post).

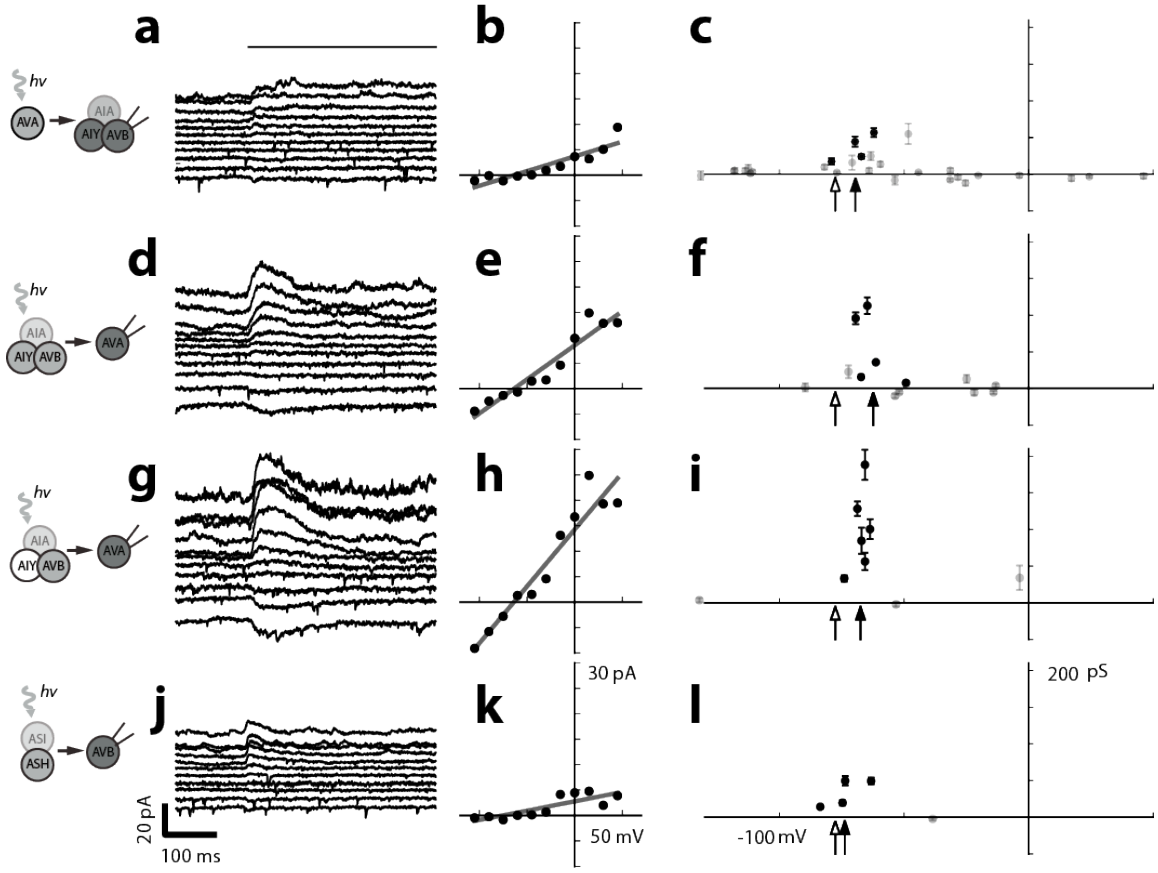

Figure 3. Biophysical properties of the functional connectivity amongst the neurons AVA,AVB and ASH (**a**) Voltage clamp recordings of an AVB neuron held at family 11 of holding potentials ranging from -115mV to 45mV. Synaptic currents were evoked when *rig-3* expressing neurons were photo-simulated with blue light (bar, top). (**b**) The average light-evoked currents shown in **a** plotted against the holding potential. A linear fit (grey line) was used to estimate the conductance (slope) and reversal potential (zero-current intercept). (**c**) Estimates of conductance plotted against reversal potential for 33 preparations in which connectivity between AVA(pre) and AVB(post) was tested as in **a** and **b**. Connections with a conductance significantly different than 0 S are shown in black, (Bonferroni corrected alpha = 0.0015) and were used to calculate the group-wise average reversal potential (black arrow). Preparations with a non-significant synaptic conductance are shown in grey. The equilibrium potential for chloride (open arrow) is shown for reference. (**e-f**) Same design as **a-c** except recordings tested connectivity between *sra-11* expressing neurons and AVA. n= 14 in **f**, alpha = 0.0036. (**g-i**) same as **e-f** except recordings were performed in worms with a mutation (mg158) in the *ttx-3* gene. n= 8 in **i,** alpha = 0.006 . (**j-l**) Connectivity between ASH and AVB. n=5 in **l**, alpha = 0.001. The the synaptic connectivity being tested in each row of panels is shown by the cartoon on the left with darker coloration indicating greater levels of transgenic protein expressed by the indicated neuron.

We next sought to test for the reciprocal connection - AVB(pre) to AVA(post) - using an analogous approach as we used for the AVA(pre) to AVB(post) connection. In this

instance we expressed ChR2 using the *sra-11* promotor and tdTomato using the *nmr-1* promotor[48], again in a *lite-1*(ce314) background. This allowed us patch clamp AVA(pre) and photo-activate AVB(post). It should be noted, however, in this case additional neurons — primarily AIY(L) and AIY(R) — were also likely activated by our photosimulation light.

Photostimulation of the *sra-11* expressing neurons evoked synaptic currents (Fig. 3d), in AVA(post) in 5/15 preparations (Fig. 3e,f). Using the exclusion approach described above, we estimated the reversal potential of the currents to be -62.4±3.56 mV amongst preparations with a statistically significant conductance. These results suggested the presence of inhibitory functional connectivity between AVB(pre) and AVA(post), however the more promiscuous expression pattern of the *sra-11* promotor potentially confounds our interpretation of this result. AIY represents a particularly problematic confound because previous studies have suggested that activity in AIY serves to promote forward locomotion [57,85,124]. Thus, it is natural to think that AIY may send inhibitory connectivity to the reverse command neurons AVA.

To rule out the possibly that the light-evoked synaptic currents we observed in AVA(post) resulted entirely from AIY activation, we took advantage of mutations (mg158) in the *ttx-3* gene that is required for the expression of *sra-11* in AIY. [120] We expressed *sra-11*::ChR2::YFP and *nmr-1*::tdTomato in a *ttx-3*(mg158) background and found that as expected, ChR2::YFP expression in AIY was eliminated (not shown); however, the light evoked inhibitory synaptic currents persisted in AVA(post) in 6/10 preparations (Fig. 3g-i). Furthermore, the reversal potential (-67.49±1.48 mV) of these currents was not altered in a major way (Fig. 3i). This suggests that

synaptic output from AIY is at most a minor component of the net connectivity from *sra-11* expressing neurons and AVA(post).

Presently, we have not ruled out a possible contribution of synaptic output from AIA to AVA, however, we find that AIA is an unlikely source of the majority of the light-evoked synaptic currents for three reasons: (1) ChR2 is expressed weakly in AIA when compared to AVB [120]. (2) Unlike AVB, there are no monosynaptic contacts from AIY onto AVA [41]. (3) the *ttx-3* mutation weakens the expression of *sra-11* reporters in AIA [120].

AVA and AVB neurons receive bi-directional regulation from the ASH nociceptor

When a worm is crawling in the forward direction and its nose encounters an aversive stimulus, the worm responds rapidly and reliably with a bout of reverse locomotion. It has been well established that the sensory neuron ASH is necessary for this avoidance response [50,62,66]. Consistent with the role of ASH in sensing aversive sitmuli, and AVA in commanding reverse locomotion, studies from our lab and others have demonstrated excitatory functional connectivity between ASH and AVA [67-69,73,78,82,118]. In spite of the well-studied interaction between ASH and the reverse command neurons, it is not known how or if ASH interacts with the forward command neuron AVB. Since activation of AVB would likely antagonize a reverse escape bout, it might be expected that functional connectivity between ASH and AVB is inhibitory if it exists, however, ASH also makes direct dyadic synapses to both AVA and AVB.[41] Following Dale's principle [125,126] it is then also reasonable to hypothesize that ASH excites AVB, since it is known that ASH releases glutamate to excite AVA[67,116,118].

Our ability to perform electrical recordings from AVB affords us the ability to determine if ASH(pre) excites or inhibits AVB(post). Thus, we used the *sra-6* promotor to express ChR2 in ASH(pre) and measured the reversal potential of light-evoked currents in AVB(post). Again we identifed AVB(post) by expressing tdTomato with the *sra-11* promotor. By photostimulating ASH(pre) we observed synaptic currents (Fig. 3j) in AVB(post) in 4/5 preparations (Fig.3k,l). These currents had a reversal potential of -73.82 ± 4.17 mV, indicating that net effect of functional connectivity between ASH and AVB is inhibition. Thus, the effect of ASH activation is bi-directional: simultaneous activation of AVA and inhibition of AVB.

Synaptic conductance noise suggests a mechanism for state transitions in a reciprocally connected neural circuit

The reciprocal connectivity demonstrated by our optogenetic experiments resembles a well studied class of oscillatory circuits known as half centers [127,128], however, analysis of *C. elegans* locomotory behavior indicates that transitions between forward and reverse locomotion are not rhythmic, rather they occur randomly [93]. Accordingly, we expect command neuron activity to also switch between activity patterns randomly rather than rhythmically.

Non-linearities and time-dependance included as terms of many existing half center models distinguishes them from the AVA and AVB circuit, especially since these terms are often critical for the limit cycle behavior of the oscillations see [129]. In contrast, as we have shown in Fig. 2, the intrinsic currents in AVA and AVB appear to be largely passive. Given the passive intrinsic properties of the command neurons, the stability of the flip–flop behavior must be generated at a network level. We hypothesized that reciprocal inhibitory connectivity alone would be sufficient to accommodate the demand for stability in the flip–flop behavior, and conductance

noise could allow for random transitions between stable states. This hypothesis generates two questions: What form and properties are required of the synaptic transfer function to meet the demand for stability? (2) Is noise is able to drive transitions without entirely overwhelming stability?

In order to answer these questions we constructed a simplified conductance model of the system, modifying an existing model of two reciprocally connected passive neurons by adding noise. The original, deterministic form of this model included two units — named a and b here — that were described by their capacitive properties, a single passive leak conductance and an inhibitory synaptic conductance that coupled the units via an instantaneous sigmoidal transfer function [129]. In this model, the voltage $\vec{V} = (V_a, V_b)$ changes as a function of the conductance-driven membrane currents according to symmetrical differential equations for V_a and V_b such that such that for a:

$$\frac{dV_a}{dt} = \frac{-I_{al} - I_{b\to a}}{C_m}$$

Where I_{al} is the leak current in a, $I_{b\to a}$ is the synaptic current in a coming from b, and C_m is the membrane capacitance. The synaptic current, $I_{b\to a}$ depends on the driving force on chloride and the synaptic conductance so that

$$I_{b\to a} = \bar{g}_s g_{b\to a}(V_a - E_{Cl})$$

Here E_{Cl} is the equilibrium potential for chloride, $\bar{g}_s$ is a general synaptic conductance scaling that is shared by all synaptic terms in the model. The synaptic transfer function $g_{b\to a}$ is a sigmoidal function of the voltage in b and ranges from zero to one:

$$g_{b\to a} = \frac{1}{1 + e^{\beta(U - V_b)}}$$

where U is the half-maximal activation voltage of the synapse and β is the gain.

This description conforms well to our experimental observations of the passive intrinsic properties of AVA and AVB (Fig. 2a,b) and inhibitory reciprocal synaptic connectivity (Fig. 3a–i). We modified these deterministic equations to introduce noise into the leak term. Because of the large amount of ongoing synaptic activity and relatively depolarized zero-current potential of the AVA and AVB neurons (Fig. 2a,b) we assumed a leak conductance that was the sum of ongoing excitatory and inhibitory synaptic input [130] $I_{al} = I_{ae} + I_{ai}$.

To simulate the perturbation noise we used a form of colored noise known as an Ornstien-Uhlnbeck (OU) process [131]. This stochastic process has a stationary mean and properties that are known analytically, therefore the process can be described entirely by the standard deviation, σ_{cond}, of excursions from the mean and the autocorrelation time constant τ_{cond}. Furthermore, an OU process has been shown to approximate the synaptic conductance waveform resulting from the non-saturating sum of large numbers of synaptic inputs with Poisson release statistics and a unitary waveform with an instantaneous rise and exponential decay. Therefore we added independent OU processes, X_{ae} and X_{ia} to the conductance driving the both leak currents such that in a

$$I_{ae} = (\bar{g}_s + X_{ae})(V_a - E_0)$$
$$I_{ai} = (\bar{g}_s + X_{ai})(V_a - E_{Cl})$$

where E_0 is the equilibrium potential for a nonselective cation channel.

Through power spectrum analysis it can be shown that the time constant of the exponential decay of the unitary inputs provides the autocorrelation time constant for the corresponding OU equations [132]. Accordingly, we used the decay time-constant taken from recordings of miniature synaptic currents recorded from AVA

and AVB (Fig 2a,b) to set τ_{cond}. We then varied the σ_{cond} to probe how the system responded to increasing levels of noise. In cases when σ_{cond} of the noise process is set to zero, our model reduces to the deterministic form described by Manor and colleagues [129].

As was previously shown, depending on the choice of parameters, the deterministic form of our model may exist in a configuration with three steady-state solutions. In this configuration two of the steady-state solutions are stable and one is unstable. The stable solutions have the underlying neurons, a and b at unequal membrane potentials, whereas the unstable solution has a and b at equivalent membrane potentials. We found that using values of membrane capacitance, input resistance and synaptic conductance on the same order as we observed in AVA and AVB, the three steady-state configuration was possible so long as appropriate parameters of the synaptic transfer function were chosen (Fig. 4a). If the transfer function has low gain, or the threshold is outside a range of critical values, only a single steady-state solution exists (Fig. 4b,c).

We first assumed a synaptic transfer function that allows for a three-solution space, and asked if noise might be sufficient to drive transitions between stable solutions. After increasing σ_{cond} of the noise to a critical level (not shown), we found that $\vec{V}$ exhibited flip-flop behavior (Fig. 4d).

To better understand the mechanisms underlying the formation and transitions of the flip-flop, we analyzed the behavior of the stochastic form of the model with respect to the state space of the deterministic form. This analysis is justified by the fact that the nose term has a zero mean, and τ_{cond} is fast (0.5ms) compared to the membrane time constant (~2ms). Thus, the deterministic state-space represents an approximation of the average behavior of the stochastic system. In Fig. 4e we plotted the trajectory of the simulation shown in Fig. 4d on the state space shown in Fig. 4a.

This analysis demonstrates that the two stable steady-state solutions in state space form the basis for the two stable voltage configurations during the flip-flop behavior. This analysis also ads insight into the time-course of the transitions. It can be seen that because of the nature of the derivative field, when transitions occur, they progress through the low magnitude derivative field around the unstable steady-state solution. This has an important consequence: since the transition region roughly follows a diagonal with a negative slope, transitions appear as simultaneous changes in both neurons i.e. the hyperpolarized unit begins to depolarize at the same time as the depolarized unit begins to hyperpolarize.

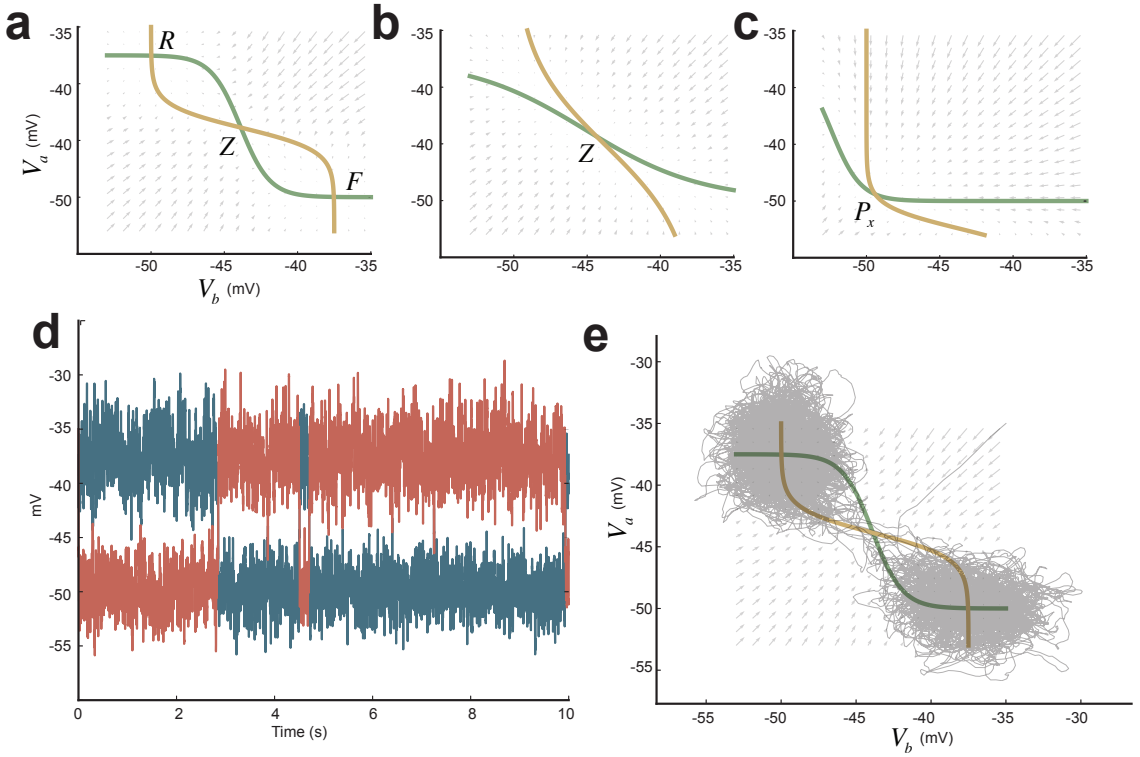

Figure 4. Conductance model of reciprocally inhibited passive neurons (**a-c**) state space and vector field (arrows) of the time derivatives for the state variables V_a and V_b, given various parameters of the synaptic transfer functions. The the V_a nullcline is plotted in yellow, V_b in green. (**a**) Three steady-state solutions are present when the transfer function has high gain, β, and an intermediate threshold value, U. The points labeled F and R are stable whereas Z is unstable. (**b**) The same U values are used as in **a** except β of the functions are increased. In this case a single stable steady-state solution, Z exists. (**c**) Solutions when the high β transfer functions in **a** have more negative U, here a single steady-state solution P_x exists. (**d**) The voltage time-series of the a (red) and b (blue) units resulting from a simulation where noise was added to the conductance terms. The parameters of the U and β were the same is in **a**. (**e**) The path of the system in **d** plotted on the state-space given in **a**. Initial conditions in **d** and **e** have $V_a = V_b =$ 0mV.

Threshold noise provides a novel mechanism for state transitions in a flip-flop circuit

A critical assumption we made in this model was the selection of a synaptic transfer function that is static, and generates the three-steady-state solutions. This assumption is not necessarily justified. In the event parameters of the synaptic transfer functions are chosen that yield single steady-state solutions as in Fig. 4b&c, the addition of conductance noise simply results in $\vec{V}$ fluctuating around the steady-state solutions(not shown). A more interesting situation arises when we consider the possibility that the transfer function itself is subject to random fluctuations that alter the relationship between the voltage in the neuron and the amount of transmitter released.

Many biologically plausible processes might account for such fluctuations or noise in a transfer function. One source of such noise that may be particularly applicable to *C. elegans* synapses is the random opining and closing of ion channels near the pre-synaptic density. This noise source, commonly referred to as channel noise, has been shown through theoretical and experimental work to result in fluctuations of the threshold for action potential generation [133-135]. This effect is especially pronounced in the small diameter cables of axons or neurites [136]. Since the synapses between *C. elegans* neurons are generally made *en passant,* many of the presynaptic specializations are restricted to such cylindrical neurites where channel noise may have a major influence on the voltage dependence of synaptic release. Furthermore, individual channel effects may be exacerbated in *C. elegans* since the total number of channels of a particular type expressed by an single neuron may number as low as 50 [89].

We asked what effect noise acting on a synaptic transfer function might have on the behavior of the system by adding noise X_{at} and X_{bt}, henceforth 'threshold noise', to the threshold terms of the transfer functions such that for a:

$$g_{a\to b} = \frac{1}{1+e^{\beta(X_{at}+U-V_b)}}$$

Again, we used an OU process as the noise source since it recently has been shown to approximate the behavior of a population of channels with two-state kinetics in a computationally efficient manner. In this approximation, the autocorrelation time constant τ_{thresh} of the OU process is inversely equal to the sum of the single-channel opining and closing rates [137]. Since we do not have physiological data to constrain τ_{thresh} for this process we explored the behavior of the model varying τ_{thresh} from 1ms to 3.125s.

The effect of threshold noise on the behavior of the model depended jointly on the standard deviation of the threshold noise, σ_{thresh} as well as τ_{thresh} (Fig. 5). In cases where τ_{thresh} was fast, the effect of threshold noise was similar to the effect of conductance noise: at small σ_{thresh} the system tended to dwell in a single state; at high σ_{thresh} the system was overwhelmed by the noise; at intermediate values the system displayed flip-flop behavior, switching between two states F and R.

In the case that τ_{thresh} was slow, two new states emerged, these consisted of one state in which both neurons were hyperpolarized, P_x, and another in which both neurons were depolarized, P_y (Fig. 6a). This had a surprising effect on the nature of the flip-flop behavior. Transitions between the two one-on, one-off configurations,

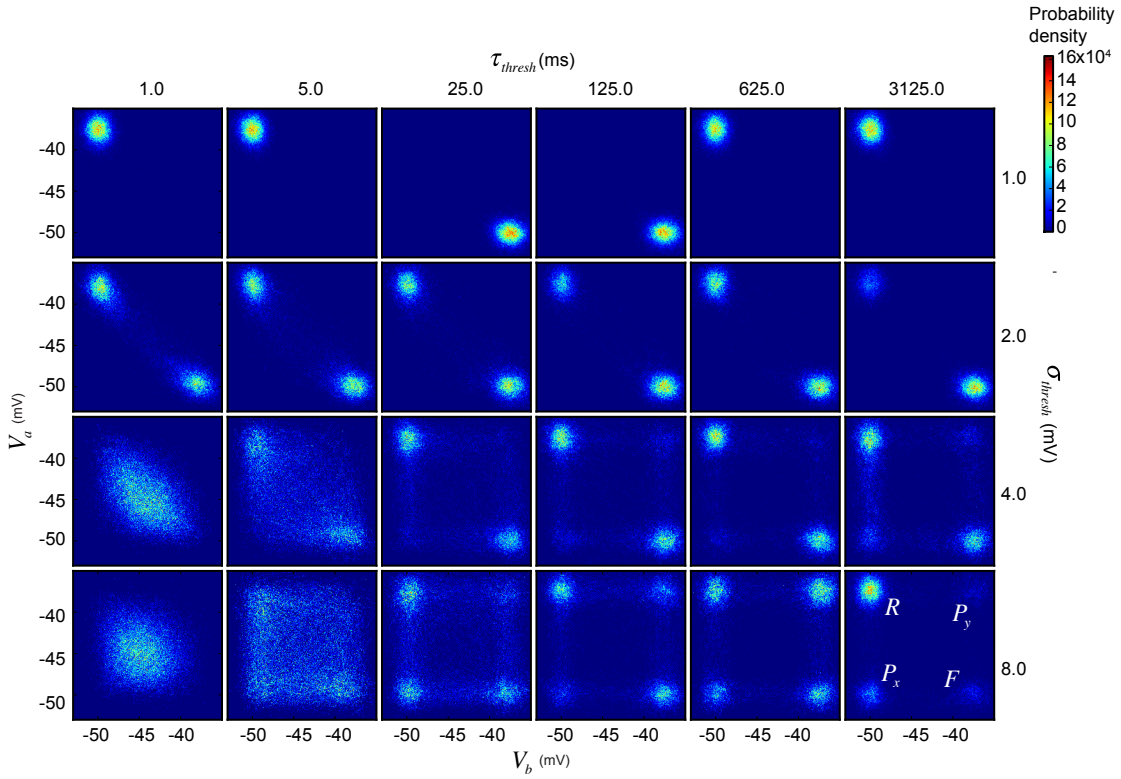

Figure 5. Effect of adding threshold noise to the distribution of voltages in a model flip-flop circuit. Matrix of two-dimensional occupancy histograms show the probably density for voltage vectors $\vec{V} = (V_a, V_b)$ generated from 30s of simulated data. Columns show simulations with identical threshold noise autocorrelation time constants, τ_{thresh} (ranging from 1.0 to 3125ms). Rows show simulations with identical threshold noise standard deviations σ_{thresh} (ranging from 1.0 to 8.0 mV). Note that when a value of σ_{thresh} of 1.0 mV is used, the system dwells for the entire simulation around a single configuration (F or R). Also note that short τ_{thresh} tended to yield simulations in which noise overwhelmed the system. In the simulations shown here where σ_{thresh} was 4.0 mV or larger, a four state regime emerged, with the system visiting the P_x and P_y configurations in addition to F and R. Blues indicate low probability density, yellows and reds indicate high density. To improve visual clarity conductance noise with a standard deviation, σ_{cond}, of 20pA was included in all simulations (see Fig. 7). The regions in state-space corresponding to the four states (F, R, P_x, P_y) are labeled in the bottom right hand histogram.

(F , R) now appeared in which one of the new states (P_x, P_y) served as an intermediary (Fig. 6a).

State-space analysis again helps understand the emergent behavior of the system. Because the two new states form when threshold τ_{thresh} is slow compared to the membrane time–constant we may apply a quasi-steady-state assumption to our analysis; when τ_{thresh} is slow, at any time-point, the instantaneous dynamics of the system are approximated by a phase-space that takes into account the values of the noise terms at that instant.

In Fig. 6b,c we plot the nullclines and fixed points that are formed using values of X_{at} and X_{bt} taken from time-points when the system is in P_x or P_y. From this view it can be seen that single steady-state solutions corresponding to the P_x and P_y conditions result when both thresholds simultaneously deviate in the negative or positive direction. In this case, floor and ceiling effects dominate, and changes in the membrane potential no longer result in changes in transmitter release; thus the reciprocal synapses become either tonically active or tonically inactive, and the system is drawn to the newly formed stable fixed point.

The solutions for the P_x and P_y states can be derived analyticity by setting the synaptic conductance terms to either zero or one in the model equations (see methods), and thus provide an explanation how fluctuations in the threshold can lead to the system occupying these new states. Notably, when threshold noise is applied, the canonical F and R states may still form in situations when the nullclines assume a configuration with two stable solutions (Fig. 6d). However, formation of a P_x or P_y state can break the system out of these stable F or R states, potentially catalyzing transitions between F and R.

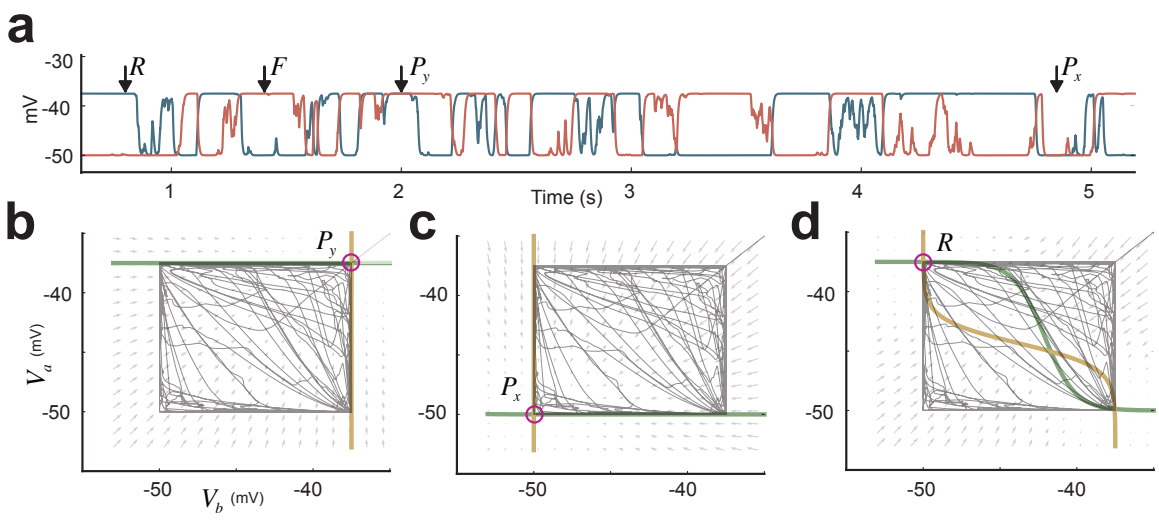

Figure 6. Simulated behavior of reciprocally inhibited passive neurons when the synaptic thresholds are subject to noise. (**a**) Voltage time-series for the a (red) and b (blue) units. The system dwells preferably in four configurations indicated by the arrows. At point R, a is depolarized and b is hyperpolarized. The opposite situations exists at point F. At P_y and P_x, a and b are either co-hyperpolarized or co-depolarized, respectively. (**b-d**) the state-space produced when values of the noise terms at the P_y, P_x and R time-points (**b,c,d** respectively) shown in **a** are applied to the threshold. The path of the system (grey lines) from the simulation shown in **a** is plotted on each panel as a reference. The location of the system at the given time-point is indicated with a magenta circle.

DISCUSSION

We probed the functionality of hypothetical circuitry responsible for controlling *C. elegans* locomotory behavior using a combination of whole cell electrophysiology and optogenetics. We first examined the intrinsic properties of the command neurons AVA and AVB and found them to be predominantly passive. Next we examined putative connectivity between the command neurons for forward and reverse locomotion and found evidence for reciprocal inhibition. We then showed that the nociceptor ASH regulates locomotion by inhibiting the forward command neuron AVB, in addition to its known role exciting the reverse command neuron AVA [73,82,118]. Finally we developed a model of passive reciprocal inhibition that is sufficient to account for the flip-flop behavior of the *C. elegans* command neurons.

Intrinsic properties of the command neurons

Using whole cell voltage clamp recordings of the AVB neuron class we discovered that the kinetics and current-voltage relationship of AVB membrane currents were primarily passive, and in close agreement with those previously recorded in the reverse command neurons AVA.

Because of the invasive nature of the recording procedure, our estimation of whole cell currents are necessarily prone to some uncertainty. Of particular concern is the shunting effect of the leak conductance around the electrode seal, and the washout of cytosolic contents following whole cell access. Whereas we cannot rule out the possibility that these difficulties cause us to miss regenerative currents that would be sufficient to generate bi-stability in either AVA or AVB, we feel this is unlikely since we are able to identify these types of regenerative currents in other *C. elegans* neurons such as ASH (Fig. 2C). Consequently, the intrinsic regenerative currents of the command neurons must be unusually susceptible to the whole cell procedure, or the the intrinsic currents are largely passive. We find the latter explanation more parsimonious.

Reciprocal inhibitory synaptic connectivity

Our ability to identify and patch-clamp AVB expands the repertoire of neurons accessible to electrical recordings to both classes of major locomotory command neurons. This presented the prospect of studying the synaptic interactions between these neurons by combining optogentics with electrophsiology. Unfortunately, this approach requires that optogenetic photostimulation light is delivered broadly to the neurons in the head. Thus, the expression system we use to drive ChR2 in presynaptic members of a putative coupled pair requires a greater degree of specificity than the system used to label the postsynaptic member.

The *rig-3* promotor allowed us to express ChR2 in AVA, allowing straightforward testing of AVA(pre) to AVB(post) connectivity. The situation was more complicated, however, when testing for the reciprocal connection - AVB(pre) to AVA(post). This is because the most specific promotor for AVB also drives expression in the interneurons AIY and AIA. Fortunately, we were able to use a mutation in the *ttx-3*(mg158) gene to control for the effect of AIY(pre) on this connection. The possibility of a confound from synaptic output of the AIA(pre) neuron remains. Nevertheless, we believe that connectivity between AIA(pre) and AVA(post) if it were to exist, would unlikely reverse our conclusion of inhibitory connectivity between AVB(pre) and AVA(post). This is because weaker ChR2 expression in AIA, and anatomical evidence of numerous monosynaptic contacts from AVB(pre) onto AVA(post) favors the *a priori* interpretation of a strong AVB(pre) to AVA(post) connection that dominates the observed currents.

Dissection and exposure of the command neuron somata is unfortunately a necessary requirement of the whole cell recording procedure. Although we take steps to minimize the invasiveness of the procedure, the synaptic connectivity of the network is likely disrupted to some extent by dissection. We expect that the large variability in conductance values between different preparations is due to this disruption, however, other possibilities exist such as day-to-day variation in the laboratory environment or individual differences in the life history of the worms.

To control for preparation-to-preparation variability in our estimate of synaptic reversal potentials, we only included trials in which a statistically significant synaptic conductance was measured. This is based on the notion that we are better able to estimate the true reversal potential of a connection from a preparation that yields a

large, easily detectible synaptic signal than one that yields a small signal. Unfortunately, this approach makes it difficult to make comparisons regarding the magnitude of the conductance between groups since we are using conductance itself as an exclusion criterion. Nevertheless, it is interesting to note that a much larger proportion of the group testing connectivity from AVB(pre) to AVA(post) displayed a significant conductance than group testing AVA(pre) to AVB(post). This is consistent with the wiring diagram which shows fewer contacts from AVB(pre) to AVA(post) than in the reciprocal direction, and may underly the reason that freely crawling worms spend more time crawling forward than reverse[41].

Flip-flop circuit for locomotory control

A possible role of reciprocal cross connectivity between the command neurons might be to help stabilize segregated membrane potentials in the command neurons, generating a flip-flop configuration such that one neuron is active while the other is inactive. Two reciprocally inhibited neurons is usually referred to as a half center [127] and has been the subject of extensive theoretical investigation regarding the generation of rhythmic oscillations. Whereas half-centers are clearly capable of driving rhythmic processes, they have received less study with regards to the production of random switching between stable states, as is observed in worm locomotory behavior [9].

It has been shown that a simple conductance model of a half center with passive neurons is sufficient to produce an oscillator of two neurons with anti-phase activity patterns [129]. We asked if noise could drive flip-flop behavior in a similar model.

The cell-intrinsic and synaptic conductance terms in our model were taken to have no time dependence. Whereas we took this simplification to make the system easier

to analyze, it is partially supported by the fact that the underlying cell-intrinsic and synaptic currents shown in Fig. 2 and Fig. 3 respectively, have only moderate time dependance. Ultimately, the kinetics of the currents likely play an important functional role in the behavior of the actual command circuit, we nevertheless find that they are not required for the production of stable states and random switching behavior in our simplified model.

An additional simplification of our model was the use of passive neurons. Beyond mere simplification however, this closely reflects our electrophysiolgical observations of roughly linear current-voltage relationships in AVA and AVB. Given the inclusion of passive neurons, a nonlinear synaptic transfer function was required to produce stable state-wise activity patterns in the two units. Presently, we have no data regarding the actual form of the transfer functions used by the reciprocal connections. Previous investigations of connectivity between other *C. elegans* neurons [72,118] have shown graded, low gain input-output functions that would be unlikely to generate the stable segregated states we observed in our model. Graded inhibitory synaptic transfer functions with steep input-output relationships have recorded in the closely related nematode *Ascaris* thus raising the possibility that similar transfer functions might be found between *C. elegans* neurons [96]. An important prediction of our model therefore, is that the reciprocal connectivity between the command neurons should have a steeper, non linear input-output functions than has been shown previously in the *C. elegans* central nervous system.

Fluctuations in the synaptic threshold may explain emergent behavioral states

The notion of the flip-flop voltage pattern as we defined it necessarily requires that a transition to a depolarized voltage in one neuron must be accompanied by a corresponding transition to a hyperpolarized voltage in the other neuron. This requirement, does not necessarily dictate the fine grain temporal sequence by which

these transitions proceed. Two hypothetical sequences exist, the first involves simultaneous transitions in both neurons, whereas the second involves one neuron making a transition which is then followed by a concomitant transition in the other neuron. We found that our model was sufficient to generate both types of sequences depending on how noise was introduced into the equations.

We hypothesized two possible ways that noise might perturb the system. The first way assumed a process driven by fluctuations in tonic synaptic input from excitatory and inhibitory neurons. This approach has been used extensively to model the effect of background conductance noise on neural computations [132]. This source of noise was sufficient to generate flip-flop transitions that were realized as simultaneous changes in both neurons.

The second way we introduced noise into our model was through fluctuations in threshold of the synaptic transfer functions. This source of noise has not been demonstrated experimentally, however it may result from channel noise at the presynaptic terminal. Since the statistics of this noise would be determined by the rate constants of the underlying ion channels, our model predicts that manipulation of the ion-channel rate constants should alter the switching rates of the command neuron flip-flop and, thus the locomotory behavior of the worm in a predictable way. This prediction is potentially testable given the identification of mutant alleles of ion channel genes known to localize to presynaptic regions [138-142].

To our knowledge the theoretical consequences of such random fluctuations of synaptic threshold on the behavior of a neural circuit has not been examined. We find the possibility of threshold noise especially compelling with respect to the *C. elegans* command neuron circuit since it provides a mechanism to generate a critical aspect of worm locomotory behavior. High temporal resolution analysis of

worm locomotion has has shown that in addition to bouts of forward and reverse crawling, worms will stop for brief periods of time before resuming in either the forward or reverse direction [114]. These pause states might very well arise as a consequence of threshold noise.

It is easy to imagine a linear relationship in which the crawling velocity of a worm is simply a scaled version of the voltage difference between its forward and reverse command neurons. Given this transformation, our simulations would produce very different results depending on whether a conductance or threshold noise source is used. In the case that conductance noise is dominant, worm velocity would reside predominantly in either a forward or reverse mode (Fig. 7a) with relatively broad distributions. In contrast, in the case that threshold fluctuations dominate, then three velocity modes (forward, reverse and stopped) would be observable from whole worm behavior (Fig. 7b). A hybrid situation is also possible, in which both conductance and threshold variations are involved. In this case, we would expect a broad tri-modal distribution of velocity values (Fig. 7c). The voltages of the actual command neurons during the pause events are unknown, but future studies taking advantage of new voltage imaging technologies might be able to answer this question.

Bi-directional sensory regulation of locomotion

Another opportunity afforded by the ability to perform electrical recordings from AVB was the prospect of extending our understanding of sensory regulation of the command circuit beyond the known synaptic connectivity with AVA, to possible inputs on AVB. We found that photoactivating nociceptive neuron ASH evoked inhibitory synaptic currents in AVB. This is in contrast with the excitatory effect ASH activation has on AVA.

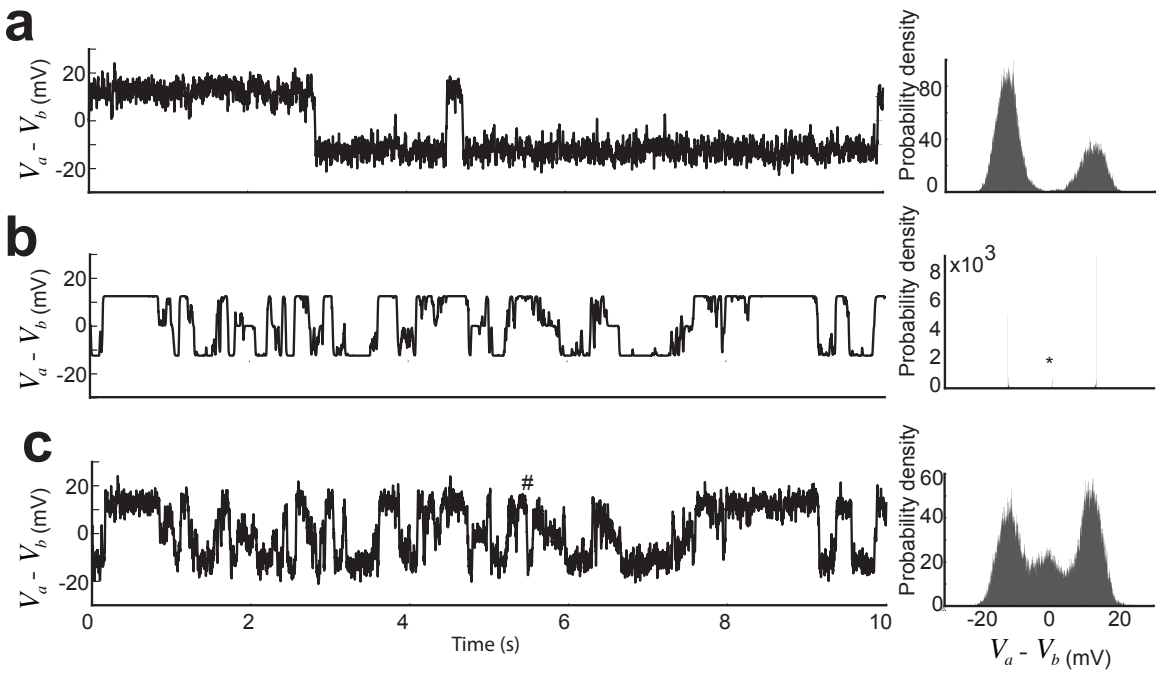

Figure 7. Hypothetical velocities generated from the voltage differences between reciprocally inhibited model neurons. (**a**) Time-series of voltage differences when only conductance noise is used. The probability density histogram of the difference values is shown to the right. (**b**) Same as in **a**, except that noise is introduced only into the synaptic threshold term. Note the narrow distributions and emergence of a third peak (asterisk) at zero (**c**) Hybrid model in which both conductance noise and threshold noise are introduced. This produces a broad tri-modal distribution. Note that transitions events not apparent in either **a** or **b** appear in **c** (pound). $V_a - V_b$ could be transformed into a vector representing velocity by multiplying by an arbitrary scalar having the units mm/(s*mV). The conductance and threshold noise waveforms from in **a** and **b** were used in **c**.

Since our investigations here also demonstrate inhibitory connections between AVA(pre) and AVB(post) it is possible that ASH generates its inhibitory effect on AVB by way of a polysynaptic pathway through AVA. Indeed, our simplified conductance model would treat an excitatory sensory input on one unit, identically to an equivalent inhibitory sensory input to the other unit. This fact results entirely from the symmetric and instantaneous nature of the synaptic transfer function we used. In reality, our model is likely an over-simplification and both synaptic delays and asymmetries play an important role *in-vivo*. Importantly, we found that the synaptic currents we recorded in AVB have roughly the same latency whether ASH and AVA

serves as the pre-synaptic neuron. This suggests that ASH and AVA inhibit AVB via pathways of equivalent length. Indeed, direct synaptic pathways from ASH to both command neurons might be functionally relevant since they could short-circuit the latency associated with reciprocal connectivity, thus accelerating the locomotory response to an aversive stimulus.

Here we have primarily studied the *C. elegans* locomotory circuit as it relates to escape behavior. It is interesting to note that in addition to escape, worms use locomotory switching to construct a number of higher order behaviors such as the search for food and mates. This implies that a large number of sensory modalities are integrated into a common behavioral switch. Therefore the command neuron flip-flop represents a general example of decision making by a noisy neural system. Indeed, several models of decision making in humans and non-human primates involve the interaction between a noisy diffusion process and the attractor dynamics of the underlying neural network [143]. Given the attractor dynamics of our simplified model, the *C. elegans* locomotory circuit may represent a system in which these theories of decision making can be examined in a genetically accessible organism.

METHODS

Strains

Animals. The strains used in this study were wild-type *C. elegans* Bristol (N2);lite-1(ce314);ntIs37[*rig-3*::ChR2::coel::GFP];ntIs35[*sra-11*::tdTomato];KyEx3801[*sra-11*::ChR2*GFP;coel::dsRed];ntIs29[*nmr-1*::tdTomato(vvtva)];lite-1(ce314); lite-1(ce314) X; ntIs27[*sra-6*::ChR2;unc-122::dsRed];ntIs36[*sra-11*::tdTomato];

KyEx3801[*sra-11*::ChR2*GFP;coel::dsRed];ntIs29[*nmr-1*::tdTomato(vvtva)];*ttx-3*(mg158) X.

Electrophysiology

Electrophysiological procedures generally follow those previously [118]. Briefly, recording pipettes were pulled and pressure-polished to achieve resistances of 10–20 MΩ when filled with normal internal saline. Voltage and current-clamp recordings were made with a modified Axopatch 200A amplifier. Pulses used to calculate whole-cell capacitance and series resistance were filtered at 50 kHz and sampled at 125 kHz. Voltage clamp current families, and recordings of photostimulation-evoked events, were filtered at 2 kHz and sampled at 10 kHz.

Physiological solutions. Internal saline consisted of (in mM): 143 K-gluconate , 1 CaCl2,, 4 NaCl, 1 MgCl2, 10 HEPES, 10 EGTA, pH 7.2 (KOH). External saline consisted of 5 KCl, 10 HEPES, 8 CaCl2, 143 NaCl, 30 glucose, pH 7.2 (NaOH).

Parameters of the flip-flop conductance model

The voltage V_a, V_b of two neurons a and b respectively were described by symmetrical equations governed entirely by synaptic currents. We set C_m to 1 pF, a value consistent with the measured capacitance of AVA or AVB in vivo. The chloride equilibrium potential (-75mV) and the reversal potential of a non-selective cation conductance (0mV) were used for E_{Cl} and E_o respectively. To simplify the equations, a single synaptic conductance scaling term $\overline{g}_s$ was set to 200pS and used for all currents. Whereas future studies might yield accurate estimations of the conductance for all relevant inputs to the command neurons, this value is roughly compatible with our observations from recordings of AVA and AVB; it is on the same order as the magnitude of the reciprocal conductances (Fig. 3a,b), and yields an average resting

input resistance of 1.6 - 2.5 GΩ depending on the activation of the synaptic conductance. This was intentionally higher than the 1-2 GΩ measured experimentally because we expect the act of recording from delicate *C. elegans* neurons decreases their input resistance.

The voltage equations were coupled by a synaptic conductance that was a sigmoidal function of the voltage in the alternate neuron. The gain, β, of the transfer function was set arbitrarily to 1.0 mV^{-1} and a value of 43.75 mV was used for the half maximal activation, U, since this is the voltage value half-way between the steady-state values of V_a and V_b when X_{at} goes to ∞ or -∞, (see below).

The voltage equations were integrated numerically using the Euler method with an integration time step Δt of 1μs. Noise was generated using an Ornstien-Uhlnbeck process, in which the stochastic variables X_j were updated numerically using the following rule[144]:

$$X_j(t+\Delta t) = X_j(t)e^{-\Delta t/\tau} + n\sqrt{2\sigma^2(1-e^{-2\Delta t/\tau})/2}$$

where $j \in \{at, bt, ai, ae, bi, be\}$, n was a sample from a unit normal distribution and σ and τ are the desired standard deviation and autocorrelation time constant respectively.

The nullclines for the voltage equations can be determined by setting dV_a/dt and dV_b/dt to zero. Thus $dV_b/dt = 0$ when

$$V_a = \frac{E_0 + E_{Cl} + g_{b\to a}E_{Cl}}{2 + g_{b\to a}}$$

Since $g_{b\to a}$ $g_{a\to b}$, are sigmoidal functions that goes from zero to one, they are saturated when X_{at} X_{bt} go to ∞, and thus $V_a = V_b = (E_0 + 2E_{Cl})/3 = -50.0$ mV. Similarly, when X_{at} X_{bt} go to –∞ $V_a = V_b = (E_0 + 2E_{Cl})/3 = -37.5$ mV. For this reason in our simulations we set the average synaptic threshold, U to -43.75 mV, half-way between these values to provide for symmetrical solutions.

CHAPTER IV

SUMMARY

In this dissertation we sought to identify the synaptic connectivity and circuit mechanisms that are responsible for selecting between two simple behavioral motifs in the nematode *C. elegans*. We first developed methodology that allowed us to probe the nervous system of this simple organism by combining the new transgenic technique of optogenetics with traditional electrophysiology. We first applied this approach to study the synaptic connectivity between the sensory neurons involved in escape behavior ASH, and the major command neurons for reverse locomotion AVA. After identifying the detailed properties of the excitatory connectivity between the escape sensory neurons and the reverse command neurons, we extended our studies to study the circuitry between ASH and the command neuron for forward locomotion AVB. Here we found inhibitory connectivity suggesting bi-directional control of the command neuron circuit by ASH. Finally, we investigated the connectivity between the command neurons AVA and AVB and found evidence for reciprocal inhibition.

We used the circuit motif discovered in our experiments to develop a model that was sufficient to predict many aspects of spontaneous and sensory-evoked locomotory switching behavior observed in crawling *C. elegans*. Furthermore, the model suggested that the decision making algorithm employed by worms during locomotory switching may be described according to the dynamics of a brownian particle in a free-energy, or attractor space. This view of *C. elegans* behavior is compliant to several generalized theories of decision making that utilize a framework of statistical mechanics or chemical kinetics [143]. Thus, the locomotory circuit we identified here may provide a practical testbed for concepts related to decision making in other species.

REFERENCES CITED

1. Botvinick, M. M. Multilevel structure in behaviour and in the brain: a model of Fuster's hierarchy. *Philosophical Transactions of the Royal Society B: Biological Sciences* **362**, 1615–1626 (2007).

2. Briggman, K. L. & Kristan, W. B. Multifunctional pattern-generating circuits. *Annu. Rev. Neurosci.* **31**, 271–294 (2008).

3. Prescott, T. Action selection. *Scholarpedia* **3**, 2705 (2008).

4. Torres-Oviedo, G. & Ting, L. H. Muscle synergies characterizing human postural responses. *J. Neurophysiol.* **98**, 2144–2156 (2007).

5. Bizzi, E., Mussa-Ivaldi, F. A. & Giszter, S. Computations underlying the execution of movement: a biological perspective. *Science* **253**, 287–291 (1991).

6. Glimcher, P. W. The neurobiology of visual-saccadic decision making. *Annu. Rev. Neurosci.* **26**, 133–179 (2003).

7. Fusi, S., Asaad, W. F., Miller, E. K. & Wang, X.-J. A neural circuit model of flexible sensorimotor mapping: learning and forgetting on multiple timescales. *Neuron* **54**, 319–333 (2007).

8. Ramirez, J. M. & Pearson, K. G. Generation of motor patterns for walking and flight in motoneurons supplying bifunctional muscles in the locust. *J. Neurobiol.* **19**, 257–282 (1988).

9. McCormick, D. A. Neuronal networks: flip-flops in the brain. *Current Biology* **15**, R294–6 (2005).

10. Kiehn, O. Plateau potentials and active integration in the 'final common pathway' for motor behaviour. *Trends in Neurosciences* **14**, 68–73 (1991).

11. Major, G. & Tank, D. Persistent neural activity: prevalence and mechanisms. *Current Opinion in Neurobiology* **14**, 675–684 (2004).

12. Llinás, R. R. The intrinsic electrophysiological properties of mammalian neurons: insights into central nervous system function. *Science* **242**, 1654–1664 (1988).

13. Hartline, D. K., Russell, D. F., Raper, J. A. & Graubard, K. Special cellular and synaptic mechanisms in motor pattern generation. *Comp. Biochem. Physiol. C, Comp. Pharmacol. Toxicol.* **91**, 115–131 (1988).

14. Alaburda, A., Perrier, J.-F. & Hounsgaard, J. Mechanisms causing plateau potentials in spinal motoneurones. *Adv. Exp. Med. Biol.* **508**, 219–226 (2002).

15. Russo, E. & Constanti, A. Topiramate hyperpolarizes and modulates the slow poststimulus AHP of rat olfactory cortical neurones in vitro. *Br. J. Pharmacol.* **141**, 285–301 (2004).

16. Brody, C. D., Romo, R. & Kepecs, A. Basic mechanisms for graded persistent activity: discrete attractors, continuous attractors, and dynamic representations. *Current Opinion in Neurobiology* **13**, 204–211 (2003).

17. Klink, P. C., van Wezel, R. J. A. & van Ee, R. United we sense, divided we fail: context-driven perception of ambiguous visual stimuli. *Philosophical Transactions of the Royal Society B: Biological Sciences* **367**, 932–941 (2012).

18. Wheatstone, C. On some remarkable and hitherto unobserved phenomena of binocular vision. *Philosophical Transactions of the Royal Society of London* **53**, 2311–2315 (1838).

19. Tong, F., Meng, M. & Blake, R. Neural bases of binocular rivalry. *Trends Cogn. Sci. (Regul. Ed.)* **10**, 502–511 (2006).

20. Pearson, J., Tadin, D. & Blake, R. The effects of transcranial magnetic stimulation on visual rivalry. *J Vis* **7**, 2.1–11 (2007).

21. Barker, A. T., Jalinous, R. & Freeston, I. L. Non-invasive magnetic stimulation of human motor cortex. *Lancet* **1**, 1106–1107 (1985).

22. Sheinberg, D. L. & Logothetis, N. K. The role of temporal cortical areas in perceptual organization. *Proc. Natl. Acad. Sci. U.S.A.* **94**, 3408–3413 (1997).

23. Leopold, D. A. & Logothetis, N. K. Activity changes in early visual cortex reflect monkeys' percepts during binocular rivalry. *nature* **379**, 549–553 (1996).

24. Wunderlich, K., Schneider, K. A. & Kastner, S. Neural correlates of binocular rivalry in the human lateral geniculate nucleus. *Nat. Neurosci.* **8**, 1595–1602 (2005).

25. Blake, R. A neural theory of binocular rivalry. *Psychol Rev* **96**, 145–167 (1989).

26. Tong, F. & Engel, S. A. Interocular rivalry revealed in the human cortical blind-spot representation. *nature* **411**, 195–199 (2001).

27. Mueller, T. J. & Blake, R. A fresh look at the temporal dynamics of binocular rivalry. *Biol Cybern* **61**, 223–232 (1989).

28. Breese, B. B. Can Binocular Rivalry be Suppressed by Practise? **6**, 686–687 *The Journal of Philosophy, Psychology and Scientific Methods* (1909).

29. Levelt, W.J. Binocular brightness averaging and contour information. *Br J Psychol* **56**, 1–13 (1965).

30. Fahle, M. Cooperation between different spatial frequencies in binocular rivalry. *Biol Cybern* **44**, 27–29 (1982).

31. Blake, R. Dichoptic reading: the role of meaning in binocular rivalry. *Percept Psychophys* **44**, 133–141 (1988).

32. Lankheet, M. J. M. Unraveling adaptation and mutual inhibition in perceptual rivalry. *J Vis* **6**, 304–310 (2006).

33. Crick, F. & Koch, C. Consciousness and neuroscience. *Cereb. Cortex* **8**, 97–107 (1998).

34. Wada, S. & Kanzaki, R. Neural control mechanisms of the pheromone-triggered programmed behavior in male silkmoths revealed by double-labeling of descending interneurons and a motor neuron. *J. Comp. Neurol.* **484**, 168–182 (2005).

35. Kanzaki, R., Arbas, E. A. & Hildebrand, J. G. Physiology and morphology of descending neurons in pheromone-processing olfactory pathways in the male moth Manduca sexta. *J. Comp. Physiol. A Neuroethol. Sens. Neural. Behav. Physiol.* **169**, 281–298 (1991).

36. Kanzaki, R. & Mishima, T. Pheromone-Triggered 'Fiipflopping' Neural Signals Correlate with Activities of Neck Motor Neurons of a Male Moth, Bombyx mori. *Zoological Science* **13**, 79–87 (1996).

37. Iwano, M. *et al.* Neurons associated with the flip-flop activity in the lateral accessory lobe and ventral protocerebrum of the silkworm moth brain. *J. Comp. Neurol.* **518**, 366–388 (2010).

38. Kanzaki, R., Nagasawa, S. & Shimoyama, I. Neural basis of odor-source searching behavior in insect brain systems evaluated with a mobile robot. *Chem. Senses* **30 Suppl 1**, i285–6 (2005).

39. Yamagata, T. *et al.* GFP labeling of neurosecretory cells with the GAL4/UAS system in the silkmoth brain enables selective intracellular staining of neurons. *Zoological Science* **25**, 509–516 (2008).

40. Takasaki, T., Namiki, S. & Kanzaki, R. Use of bilateral information to determine the walking direction during orientation to a pheromone source in the silkmoth Bombyx mori. *J. Comp. Physiol. A Neuroethol. Sens. Neural. Behav. Physiol.* **198**, 295–307 (2012).

41. White, J. G., Southgate, E., Thomson, J. N. & Brenner, S. The structure of the nervous system of the nematode Caenorhabditis elegans. *Philos. Trans. R. Soc. Lond., B, Biol. Sci.* **314**, 1–340 (1986).

42. Varshney, L. R., Chen, B. L., Paniagua, E., Hall, D. H. & Chklovskii, D. B. Structural properties of the Caenorhabditis elegans neuronal network. *PLoS Comput. Biol.* **7**, e1001066 (2011).

43. Chalfie, M. *et al.* The neural circuit for touch sensitivity in Caenorhabditis elegans. *J. Neurosci.* **5**, 956–964 (1985).

44. Chronis, N., Zimmer, M. & Bargmann, C. I. Microfluidics for in vivo imaging of neuronal and behavioral activity in Caenorhabditis elegans. *Nat. Methods* **4**, 727–731 (2007).

45. Faumont, S. *et al.* An image-free opto-mechanical system for creating virtual environments and imaging neuronal activity in freely moving Caenorhabditis elegans. *PLoS ONE* **6**, e24666 (2011).

46. Kawano, T. *et al.* An imbalancing act: gap junctions reduce the backward motor circuit activity to bias *C. elegans* for forward locomotion. *Neuron* **72**, 572–586 (2011).

47. Ben Arous, J., Tanizawa, Y., Rabinowitch, I., Chatenay, D. & Schafer, W. R. Automated imaging of neuronal activity in freely behaving Caenorhabditis elegans. *J. Neurosci. Methods* **187**, 229–234 (2010).

48. Brockie, P. J., Mellem, J. E., Hills, T., Madsen, D. M. & Maricq, A. V. The *C. elegans* glutamate receptor subunit NMR-1 is required for slow NMDA-activated currents that regulate reversal frequency during locomotion. *Neuron* **31**, 617–630 (2001).

49. Culotti, J. G. & Russell, R. L. Osmotic avoidance defective mutants of the nematode Caenorhabditis elegans. *Genetics* **90**, 243–256 (1978).

50. Kaplan, J. M. & Horvitz, H. R. A dual mechanosensory and chemosensory neuron in Caenorhabditis elegans. *Proc. Natl. Acad. Sci. U.S.A.* **90**, 2227–2231 (1993).

51. Pierce-Shimomura, J. T., Faumont, S., Gaston, M. R., Pearson, B. J. & Lockery, S. R. The homeobox gene lim-6 is required for distinct chemosensory representations in C. elegans. *nature* **410**, 694–698 (2001).

52. Pierce-Shimomura, J. T., Dores, M. & Lockery, S. R. Analysis of the effects of turning bias on chemotaxis in *C. elegans*. *J. Exp. Biol.* **208**, 4727–4733 (2005).

53. Dusenbery, D. B. Responses of the nematode Caenorhabditis elegans to controlled chemical stimulation. *J. Comp. Physiol. A Neuroethol. Sens. Neural. Behav. Physiol.* **136**, 327–331 (1980).

54. Bargmann, C. I., Hartwieg, E. & Horvitz, H. R. Odorant-selective genes and neurons mediate olfaction in *C. elegans*. *Cell* **74**, 515–527 (1993).

55. Menini, A., Hart, A. C. & Chao, M. Y. *From Odors to Behaviors in Caenorhabditis elegans*. (CRC Press: Boca Raton (FL), 2010).

56. Faumont, S., Miller, A. C. & Lockery, S. R. Chemosensory behavior of semi-restrained Caenorhabditis elegans. *J. Neurobiol.* **65**, 171–178 (2005).

57. Chalasani, S. H. *et al.* Dissecting a circuit for olfactory behaviour in Caenorhabditis elegans. *nature* **450**, 63–70 (2007).

58. Suzuki, H. *et al.* Functional asymmetry in Caenorhabditis elegans taste neurons and its computational role in chemotaxis. *nature* **454**, 114–117 (2008).

59. Albrecht, D. R. & Bargmann, C. I. High-content behavioral analysis of Caenorhabditis elegans in precise spatiotemporal chemical environments. *Nat. Methods* **8**, 599–605 (2011).

60. Ryu, W. S. & Samuel, A. D. T. Thermotaxis in Caenorhabditis elegans analyzed by measuring responses to defined Thermal stimuli. *J. Neurosci.* **22**, 5727–5733 (2002).

61. Chiba, C. M. & Rankin, C. H. A developmental analysis of spontaneous and reflexive reversals in the nematode *Caenorhabditis elegans*. *J. Neurobiol.* **21**, 543–554 (1990).

62. Sambongi, Y. *et al.* Sensing of cadmium and copper ions by externally exposed ADL, ASE, and ASH neurons elicits avoidance response in *Caenorhabditis elegans*. *Neuroreport* **10**, 753–757 (1999).

63. Hilliard, M. A., Bergamasco, C., Arbucci, S., Plasterk, R. H. A. & Bazzicalupo, P. Worms taste bitter: ASH neurons, QUI-1, GPA-3 and ODR-3 mediate quinine avoidance in *Caenorhabditis elegans*. *EMBO J.* **23**, 1101–1111 (2004).

64. Hilliard, M. A., Bargmann, C. I. & Bazzicalupo, P. *C. elegans* responds to chemical repellents by integrating sensory inputs from the head and the tail. *Current Biology* **12**, 730–734 (2002).

65. Geffeney, S. L. *et al.* DEG/ENaC but not TRP channels are the major mechanoelectrical transduction channels in a *C. elegans* nociceptor. *Neuron* **71**, 845–857 (2011).

66. Bargmann, C. I., Thomas, J. H. & Horvitz, H. R. Chemosensory cell function in the behavior and development of Caenorhabditis elegans. *Cold Spring Harb. Symp. Quant. Biol.* **55**, 529–538 (1990).

67. Hart, A. C., Sims, S. & Kaplan, J. M. Synaptic code for sensory modalities revealed by *C. elegans* GLR-1 glutamate receptor. *nature* **378**, 82–85 (1995).

68. Maricq, A. V., Peckol, E., Driscoll, M. & Bargmann, C. I. Mechanosensory signalling in *C. elegans* mediated by the GLR-1 glutamate receptor. *nature* **378**, 78–81 (1995).

69. Mellem, J. E., Brockie, P. J., Zheng, Y., Madsen, D. M. & Maricq, A. V. Decoding of polymodal sensory stimuli by postsynaptic glutamate receptors in *C. elegans*. *Neuron* **36**, 933–944 (2002).

70. Boyden, E. S., Zhang, F., Bamberg, E., Nagel, G. & Deisseroth, K. Millisecond-timescale, genetically targeted optical control of neural activity. *Nat. Neurosci.* **8**, 1263–1268 (2005).

71. Nagel, G. *et al.* Light activation of channelrhodopsin-2 in excitable cells of *Caenorhabditis elegans* triggers rapid behavioral responses. *Current Biology* **15**, 2279–2284 (2005).

72. Narayan, A., Laurent, G. & Sternberg, P. W. Transfer characteristics of a thermosensory synapse in *Caenorhabditis elegans*. *Proc. Natl. Acad. Sci. U.S.A.* **108**, 9667–9672 (2011).

73. Piggott, B. J., Liu, J., Feng, Z., Wescott, S. A. & Xu, X. Z. S. The neural circuits and synaptic mechanisms underlying motor initiation in *C. elegans*. *Cell* **147**, 922–933 (2011).

74. Liewald, J. F. *et al.* Optogenetic analysis of synaptic function. *Nat. Methods* **5**, 895–902 (2008).

75. Nagel, G. *et al.* Channelrhodopsin-2, a directly light-gated cation-selective membrane channel. *Proc. Natl. Acad. Sci. U.S.A.* **100**, 13940–13945 (2003).

76. Zhang, F., Wang, L.-P., Boyden, E. S. & Deisseroth, K. Channelrhodopsin-2 and optical control of excitable cells. *Nat. Methods* **3**, 785–792 (2006).

77. Chalfie, M., Tu, Y., Euskirchen, G., Ward, W. W. & Prasher, D. C. Green fluorescent protein as a marker for gene expression. *Science* **263**, 802–805 (1994).

78. Lee, R. Y., Sawin, E. R., Chalfie, M., Horvitz, H. R. & Avery, L. EAT-4, a homolog of a mammalian sodium-dependent inorganic phosphate cotransporter, is necessary for glutamatergic neurotransmission in *Caenorhabditis elegans*. *J. Neurosci.* **19**, 159–167 (1999).

79. Hilliard, M. A. *et al.* In vivo imaging of *C. elegans* ASH neurons: cellular response and adaptation to chemical repellents. *EMBO J.* **24**, 63–72 (2005).

80. Troemel, E. R., Chou, J. H., Dwyer, N. D., Colbert, H. A. & Bargmann, C. I. Divergent seven transmembrane receptors are candidate chemosensory receptors in *C. elegans*. *Cell* **83**, 207–218 (1995).

81. Brockie, P. J., Madsen, D. M., Zheng, Y., Mellem, J. & Maricq, A. V. Differential expression of glutamate receptor subunits in the nervous system of *Caenorhabditis elegans* and their regulation by the homeodomain protein UNC-42. *J. Neurosci.* **21**, 1510–1522 (2001).

82. Guo, Z. V., Hart, A. C. & Ramanathan, S. Optical interrogation of neural circuits in *Caenorhabditis elegans*. *Nat. Methods* **6**, 891–896 (2009).

83. Bargmann, C. I. & Horvitz, H. R. Chemosensory neurons with overlapping functions direct chemotaxis to multiple chemicals in *C. elegans*. *Neuron* **7**, 729–742 (1991).

84. Alcedo, J. & Kenyon, C. Regulation of *C. elegans* longevity by specific gustatory and olfactory neurons. *Neuron* **41**, 45–55 (2004).

85. Gray, J. M., Hill, J. J. & Bargmann, C. I. A circuit for navigation in *Caenorhabditis elegans*. *Proc. Natl. Acad. Sci. U.S.A.* **102**, 3184–3191 (2005).

86. Liu, Q., Hollopeter, G. & Jorgensen, E. M. Graded synaptic transmission at the *Caenorhabditis elegans* neuromuscular junction. *Proc. Natl. Acad. Sci. U.S.A.* **106**, 10823–10828 (2009).

87. Edwards, S. L. *et al.* A novel molecular solution for ultraviolet light detection in *Caenorhabditis elegans*. *PLoS Biol.* **6**, e198 (2008).

88. Liu, J. *et al. C. elegans* phototransduction requires a G protein-dependent cGMP pathway and a taste receptor homolog. *Nat. Neurosci.* **13**, 715–722 (2010).

89. Goodman, M. B., Hall, D. H., Avery, L. & Lockery, S. R. Active currents regulate sensitivity and dynamic range in *C. elegans* neurons. *Neuron* **20**, 763–772 (1998).

90. Lockery, S. R. & Goodman, M. B. Tight-seal whole-cell patch clamping of *Caenorhabditis elegans* neurons. *Meth. Enzymol.* **293**, 201–217 (1998).

91. Shaner, N. C. *et al.* Improved monomeric red, orange and yellow fluorescent proteins derived from *Discosoma* sp. red fluorescent protein. *Nat. Biotechnol.* **22**, 1567–1572 (2004).

92. Faumont, S. & Lockery, S. R. The awake behaving worm: simultaneous imaging of neuronal activity and behavior in intact animals at millimeter scale. *J. Neurophysiol.* **95**, 1976–1981 (2006).

93. Pierce-Shimomura, J. T., Morse, T. M. & Lockery, S. R. The fundamental role of pirouettes in *Caenorhabditis elegans* chemotaxis. *J. Neurosci.* **19**, 9557–9569 (1999).

94. Group, S. F. E. B. N. *Neurones without impulses: Their significance for vertebrate and invertebrate nervous systems*. (Cambridge University Press: 1981).

95. Davis, R. E. & Stretton, A. O. Passive membrane properties of motorneurons and their role in long-distance signaling in the nematode Ascaris. *J. Neurosci.* **9**, 403–414 (1989).

96. Davis, R. E. & Stretton, A. O. Signaling properties of Ascaris motorneurons: graded active responses, graded synaptic transmission, and tonic transmitter release. *J. Neurosci.* **9**, 415–425 (1989).

97. Richmond, J. E., Davis, W. S. & Jorgensen, E. M. UNC-13 is required for synaptic vesicle fusion in *C. elegans*. *Nat. Neurosci.* **2**, 959–964 (1999).

98. Richmond, J. E., Weimer, R. M. & Jorgensen, E. M. An open form of syntaxin bypasses the requirement for UNC-13 in vesicle priming. *nature* **412**, 338–341 (2001).

99. Burgoyne, R. D. & Morgan, A. Secretory granule exocytosis. *Physiol. Rev.* **83**, 581–632 (2003).

100. Chase, D. L. & Koelle, M. R. Biogenic amine neurotransmitters in *C. elegans*. *WormBook* 1–15 (2007).doi:10.1895/wormbook.1.132.1

101. Sieburth, D., Madison, J. M. & Kaplan, J. M. PKC-1 regulates secretion of neuropeptides. *Nat. Neurosci.* **10**, 49–57 (2007).

102. Gracheva, E. O. *et al.* Tomosyn negatively regulates CAPS-dependent peptide release at *Caenorhabditis elegans* synapses. *J. Neurosci.* **27**, 10176–10184 (2007).

103. Renden, R. *et al. Drosophila* CAPS is an essential gene that regulates dense-core vesicle release and synaptic vesicle fusion. *Neuron* **31**, 421–437 (2001).

104. Brockie, P. J. & Maricq, A. V. Ionotropic glutamate receptors: genetics, behavior and electrophysiology. *WormBook* 1–16 (2006).doi:10.1895/wormbook.1.61.1

105. Yook, K. *et al.* WormBase 2012: more genomes, more data, new website. *Nucleic Acids Res.* **40**, D735–41 (2012).

106. Macosko, E. Z. *et al.* A hub-and-spoke circuit drives pheromone attraction and social behaviour in *C. elegans*. *nature* **458**, 1171–1175 (2009).

107. Conway, B. R. & Livingstone, M. S. Spatial and temporal properties of cone signals in alert macaque primary visual cortex. *J. Neurosci.* **26**, 10826–10846 (2006).

108. Mello, C. C., Kramer, J. M., Stinchcomb, D. & Ambros, V. Efficient gene transfer in C.elegans: extrachromosomal maintenance and integration of transforming sequences. *EMBO J.* **10**, 3959–3970 (1991).

109. Goodman, M. B. & Lockery, S. R. Pressure polishing: a method for re-shaping patch pipettes during fire polishing. *J. Neurosci. Methods* **100**, 13–15 (2000).

110. Li, G.-H., Jackson, M. F. & MacDonald, J. F. Weighted least squares fitting with multiple templates for detection of small spontaneous signals. *J. Neurosci. Methods* **164**, 139–148 (2007).

111. Jones, E., Oliphant, T. & Peterson, P. *SciPy: Open source scientific tools for Python, 2001*. (2007).

112. Fujiwara, M., Sengupta, P. & McIntire, S. L. Regulation of body size and behavioral state of C. elegans by sensory perception and the EGL-4 cGMP-dependent protein kinase. *Neuron* **36**, 1091–1102 (2002).

113. Zheng, Y., Brockie, P. J., Mellem, J. E., Madsen, D. M. & Maricq, A. V. Neuronal control of locomotion in C. elegans is modified by a dominant mutation in the GLR-1 ionotropic glutamate receptor. *Neuron* **24**, 347–361 (1999).

114. Stephens, G. J., Johnson-Kerner, B., Bialek, W. & Ryu, W. S. Dimensionality and dynamics in the behavior of *C. elegans*. *PLoS Comput. Biol.* **4**, e1000028 (2008).

115. Wicks, S. R. & Rankin, C. H. The integration of antagonistic reflexes revealed by laser ablation of identified neurons determines habituation kinetics of the Caenorhabditis elegans tap withdrawal response. *J. Comp. Physiol. A* **179**, 675–685 (1996).

116. Mellem, J. E., Brockie, P. J., Madsen, D. M. & Maricq, A. V. Action potentials contribute to neuronal signaling in *C. elegans*. *Nat. Neurosci.* **11**, 865–867 (2008).

117. Lockery, S. R. & Goodman, M. B. The quest for action potentials in *C. elegans* neurons hits a plateau. *Nat. Neurosci.* **12**, 377–378 (2009).

118. Lindsay, T., Thiele, T. R. & Lockery, S. R. Optogenetic analysis of synaptic transmission in the central nervous system of the nematode *Caenorhabditis elegans*. *Nat Commun* **2**, 306–9 (2011).

119. Faumont, S., Boulin, T., Hobert, O. & Lockery, S. R. Developmental regulation of whole cell capacitance and membrane current in identified interneurons in *C. elegans*. *J. Neurophysiol.* **95**, 3665–3673 (2006).

120. Altun-Gultekin, Z. *et al.* A regulatory cascade of three homeobox genes, ceh-10, ttx-3 and ceh-23, controls cell fate specification of a defined interneuron class in *C. elegans*. *Development* **128**, 1951–1969 (2001).

121. Weidmann, S. Effect of current flow on the membrane potential of cardiac muscle. *J. Physiol. (Lond.)* **115**, 227–236 (1951).

122. Nickell, W. T., Pun, R. Y. K., Bargmann, C. I. & Kleene, S. J. Single ionic channels of two Caenorhabditis elegans chemosensory neurons in native membrane. *J. Membr. Biol.* **189**, 55–66 (2002).

123. Ramot, D., MacInnis, B. L. & Goodman, M. B. Bidirectional temperature-sensing by a single thermosensory neuron in *C. elegans*. *Nat. Neurosci.* **11**, 908–915 (2008).

124. Tsalik, E. L. & Hobert, O. Functional mapping of neurons that control locomotory behavior in *Caenorhabditis elegans*. *J. Neurobiol.* **56**, 178–197 (2003).

125. Eccles, J.C.,Fatt, P. & Koketsu, K. Cholinergic and inhibitory synapses in a pathway from motor-axon collaterals to motoneurones. *J. Physiol. (Lond.)* **126**, 524–562 (1954).

126. Strata, P. & Harvey, R. Dale's principle. *Brain research bulletin* **50**, 349–350 (1999).

127. Brown, T. G. The Intrinsic Factors in the Act of Progression in the Mammal. *Proceedings of the Royal Society B: Biological Sciences* **84**, 308–319 (1911).

128. Grillner, S. Biological pattern generation: the cellular and computational logic of networks in motion. *Neuron* **52**, 751–766 (2006).

129. Manor, Y. *et al.* Network oscillations generated by balancing graded asymmetric reciprocal inhibition in passive neurons. *J. Neurosci.* **19**, 2765–2779 (1999).

130. Destexhe, A., Rudolph, M., Fellous, J. M. & Sejnowski, T. J. Fluctuating synaptic conductances recreate in vivo-like activity in neocortical neurons. *Neuroscience* **107**, 13–24 (2001).

131. Uhlenbeck, G. & Ornstein, L. On the Theory of the Brownian Motion. *Phys. Rev.* **36**, 823–841 (1930).

132. Destexhe, A. & Rudolph, M. Extracting information from the power spectrum of synaptic noise. *J Comput Neurosci* **17**, 327–345 (2004).

133. Lecar, H. & Nossal, R. Theory of threshold fluctuations in nerves. I. Relationships between electrical noise and fluctuations in axon firing. *Biophys. J.* **11**, 1048–1067 (1971).

134. Lecar, H. & Nossal, R. Theory of threshold fluctuations in nerves. II. Analysis of various sources of membrane noise. *Biophys. J.* **11**, 1068–1084 (1971).

135. Sigworth, F. J. The variance of sodium current fluctuations at the node of Ranvier. *J. Physiol. (Lond.)* **307**, 97–129 (1980).

136. Faisal, A. A., White, J. A. & Laughlin, S. B. Ion-channel noise places limits on the miniaturization of the brain's wiring. *Current Biology* **15**, 1143–1149 (2005).

137. Linaro, D., Storace, M. & Giugliano, M. Accurate and fast simulation of channel noise in conductance-based model neurons by diffusion approximation. *PLoS Comput. Biol.* **7**, e1001102 (2011).

138. Wang, Z. W., Saifee, O., Nonet, M. L. & Salkoff, L. SLO-1 potassium channels control quantal content of neurotransmitter release at the *C. elegans* neuromuscular junction. *Neuron* **32**, 867–881 (2001).

139. Davies, A. G. *et al.* A central role of the BK potassium channel in behavioral responses to ethanol in *C. elegans*. *Cell* **115**, 655–666 (2003).

140. Kim, H. *et al.* The dystrophin complex controls bk channel localization and muscle activity in *Caenorhabditis elegans*. *PLoS Genet.* **5**, e1000780 (2009).

141. Reiner, D. J., Weinshenker, D. & Thomas, J. H. Analysis of dominant mutations affecting muscle excitation in *Caenorhabditis elegans*. *Genetics* **141**, 961–976 (1995).

142. Salkoff, L. *et al.* Potassium channels in *C. elegans*. *WormBook* 1–15 (2005).doi: 10.1895/wormbook.1.42.1

143. Deco, G., Martí, D., Ledberg, A., Reig, R. & Sanchez Vives, M. V. Effective reduced diffusion-models: a data driven approach to the analysis of neuronal dynamics. *PLoS Comput. Biol.* **5**, e1000587 (2009).

144. Gabbiani, F. *Mathematics for Neuroscientists*. (2010).